The effect of nitrogen on the cosegregation of molybdenum in a Fe-3.5wt%Mo-N(100) single crystal

Werner Albert Jordaan

2006

The effect of nitrogen on the cosegregation of molybdenum in a Fe-3.5wt%Mo-N(100) single crystal

by

Werner Albert Jordaan
B.Sc. Hons.

a dissertation presented in fulfilment of the requirements of the degree

MAGISTER SCIENTIAE

in the Faculty of Natural and Agricultural Sciences,
Department of Physics,
at the University of the Free State.

Supervisor: Prof. JJ Terblans
Co-supervisor: Prof. HC Swart
December 2006

*This dissertation is dedicated to my parents, Johan and Patricia
and my departed brother, Heinrich.*

Acknowledgements

I wish to express my sincere gratitude to:

Key Words

- Auger Electron Spectroscopy

- Segregation

- Darken Model

- Fick's Model

- Diffusion

- Iron

- Molybdenum

- Nitrogen

- Single Crystal

- Thermodynamics

Abstract

In this study the cosegregation of molybdenum and nitrogen to the (100) plane of an iron single crystal was investigated. Ternary systems are considerably more complex than binary systems in that there are seven segregation parameters to determine, as opposed to three. However, a novel approach was undertaken to minimize the amount of variables, by first analysing a similar binary system that was exposed to a nitrogen ambient. Two single crystal were selected for this purpose, i.e. a Fe-3.5wt%Mo(100) binary system and a Fe-3.5wt%Mo-N ternary system. By exposing the binary crystal to a nitrogen ambient at high temperatures it was observed that molybdenum segregated to the surface.

The segregation profiles of the two systems were acquired at constant temperatures from 797 K - 888 K and Auger Electron Spectroscopy was used to monitor the surface concentrations of the relevant species. Since accurate surface temperature measurements are essential to segregation studies, a calibrated infrared thermometer was used. The segregation profiles were generated by measuring time and the Auger signal simultaneously.

From the segregation profiles, initial estimates for the diffusion coefficients of Mo were first determined for the binary system by applying Fick's equation to the segregation profiles. From these values the pre-exponential factor, D_0, was determined to be $1.2 \times 10^{-4 \pm 2}$ m^2/s and the activation energy, E, as 258 ± 33 kJ/mol. The diffusion coefficients determined thus, were used as estimates for obtaining the Darken segregation profiles. In this case the D_0 value was found to be $2.4 \times 10^{0 \pm 1}$ m^2/s and the E value, 323 ± 16 kJ/mol. The segregation energy, ΔG, of Mo was calculated as -38 kJ/mol. In both cases it was observed that the diffusion coefficient of Mo deviated from the expected value at high temperatures due to the desorption of nitrogen from the surface. Using thermodynamic theory, an expression for the segregation energy of Mo in terms of the nitrogen surface concentration was derived. The Darken fits were repeated and it was found that the high temperature diffusion coefficient values fell on the the Arrhenius linear regression lines. For this special case, the D_0 value was calculated as $5.5 \times 10^{1 \pm 1}$ m^2/s, the E value as 345 ± 18 kJ/mol.

The segregation parameters determined for the binary system were then used as initial values for fitting the experimental data of the ternary system. Using Fick's equation, the diffusion coefficients of Mo and N in Fe were determined. From the Arrhenius linear regression, the pre-exponential factor for Mo was calculated as $3.6\text{x}10^{-2\pm1}$ m^2/s and that of N as $4.1\text{x}10^{-1\pm2}$ m^2/s. The activation energies were 308 ± 20 kJ/mol and 210 ± 40 kJ/mol for Mo and N, respectively. The segregation parameters of the ternary system were then determined via the Darken method. In this case the pre-exponential factors were $1.9\text{x}10^{-4\pm1}$ m^2/s for Mo and $2.8\text{x}10^{0\pm3}$ m^2/s for N. The activation energies were 271 ± 11 kJ/mol and 323 ± 43 kJ/mol. The segregation energy of Mo was calculated as -32 kJ/mol and for N, -19 kJ/mol. The interaction coefficient between Mo and N was calculated as -19 kJ/mol.

Contents

Chapter 1

Introduction

During the manufacturing process, metallic alloys are often heated for prolonged periods. At such high temperatures, elements of low bulk concentration (even a few ppm) have high mobilities and tend to diffuse to the surface and grain boundaries. This phenomenon is known as segregation and it can be a significant hurdle for manufacturers, since it can cause problems during welding, catalysis and strengthening, to name a few examples [1][2][3][4][5]. Segregation studies thus had its origin in finding solutions to temper embrittlement caused by grain boundary segregation and it has been extensively investigated by pioneers such as McLean [6][7]. With the advent of surface analysis techniques these studies became experimentally viable and indispensible.

Segregation is defined as the exchange of atoms between surface and bulk until equilibrium is reached. Traditionally, the concentration gradient was seen as the driving force behind segregation and equations such as that of Fick were derived [8]. However, the only parameters that one can determine via Fick's equation are the diffusion coefficients. Today, an all-encompassing thermodynamic view of segregation demands that the excess energy of the system is rather viewed as the driving force behind segregation. From this premise, the set of modified Darken differential equations can be derived. Using the Darken approach, additional parameters, namely the segregation energy and the interaction coefficients, can be calculated. It also decribes both the kinetics and equilibrium of the system unlike other theories which only describe one or the other.

3

In recent years, there has been an increased interest in multicomponent or coseg-regation. Often, it is found that non-metallic strong segregants, such as carbon and nitrogen, segregate with metals such as titanium, molybdenum and chromium which are themselves weak or non-segregating. This behaviour can be explained by an attractive interaction between the segregants. The formation of epitaxially stable, two-dimensional, surface compounds often takes place during cosegregation. A binary Fe-3,5wt%Mo system and a ternary Fe-3,5wt%Mo-N system, which has been studied by Uebing *et al* [9][10][11], were chosen as the objects of this study.

1.1 The objectives of this study

1. Determine the respective pre-exponential factors and activation energy values of molybdenum and nitrogen in iron.

2. Determine the segregation energy of Mo and N in an Fe alloy and the interaction coefficient between Mo and N.

1.2 Layout of the dissertation

Chapter 2 focuses on the theory of segregation. In this study Fick's equation and the modified Darken approach were used and are discussed extensively. Through the Darken approach, it is shown that the driving force behind segregation is the minimization of the total energy of the system and not the concentration gradient as assumed for Fick's equation. To grasp the effects of the various segregation parameters, simulations are shown as examples.

In *Chapter 3* the experimental setup is discussed. The AES system is discussed in detail and the equations for quantification are derived. In this study an infrared thermometer was used for surface temperature measurements and the calibration thereof is also discussed.

In *Chapter 4* the results of the binary and ternary systems are discussed. The diffusion coefficients and activations energies of Mo and N are determined via Fick's equation and the Darken set of differential equations and the results are compared. Using the Darken approach, the segregation energy of Mo is calculated.

In *Chapter 5* the general conclusions of this study are given.

Chapter 2

Theory

2.1 Introduction

Whenever there exists an inhomogeneous distribution of atoms or molecules within a gas, liquid or solid, the atoms move around until any concentration differences have been eliminated. This process is known as diffusion. It is a thermodynamic process and it is strongly dependent on temperature. As the temperature increases, the rate of diffusion increases exponentially. This relationship is given by the Arrhenius equation, $D = D_0\, e^{-E/RT}$, where D is the diffusion coefficient, D_0 is a constant, E is the activation energy, R is the gas constant and T is the temperature.

In the case of solids, there are two types of diffusion mechanisms, namely substitutional (or vacancy) and interstitial diffusion. As it is implied, substitutional diffusion takes place when an atom moves to a nearby vacancy position within the matrix, thus creating a new vacancy. Interstitial diffusion is the movement of atoms between interstitial sites. The two mechanisms are shown in figure 2.1. Generally, substitutional diffusion takes place for large atoms and interstitial diffusion for small ones. The activation energy is the energy that must be overcome for an atom to move from one site to another and is generally higher in the case of substitutional diffusion.

From this behaviour it is expected that a material in which the atoms are homogeneously dispersed does not exhibit any concentration changes. However, it has been found experimentally that the surface can become enriched with one or more species even if they are only impurities within the bulk. This phenomenon is known as segregation. Segregation is formally defined as the exchange of atoms between the surface and bulk until the total energy of a crystal has been minimized. It is characterized by diffusion against the concentration gradient and can take place to the grain boundaries or the surface. The latter is easier to analyze [12], but finding a correlation between the two has proven to be difficult [13].
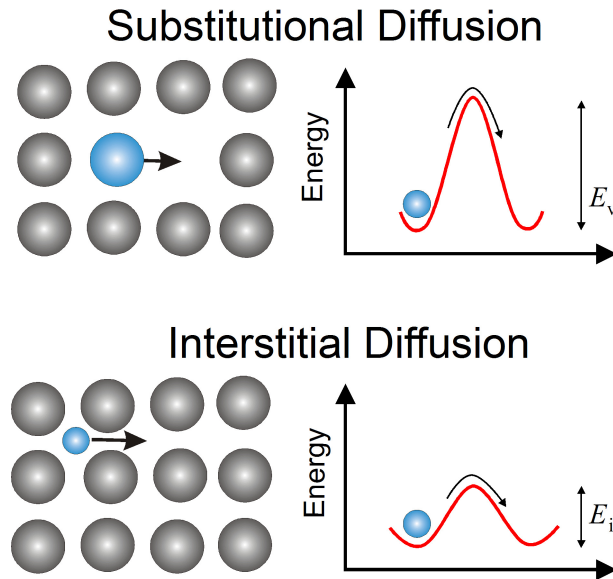
Figure 2.1: A schematical representation of substitutional and interstitial diffusion, where E is the energy the atom must overcome to move from one position to another.

There are different models that describe the equilibrium or kinetic properties of segregation. One of the earliest theories to explain binary equilibrium segregation is that of McLean [6] and for ternary systems, Guttman's equation [14], which also includes the interaction between the co-segregating species. The various segregation models are discussed extensively by Du Plessis [16]. The focus of this study leans toward the segregation kinetics and therefore Fick's equation and the modified Darken approach were used. The Darken model has proven to be quite successful and easy to apply for binary systems, but for ternary systems the amount of variables and computing power required to resolve the segregation profiles can be daunting. Therefore, Fick's equation is used to determine estimates for the diffusion coefficients which are in turn used in the Darken calculations as will be shown later.

2.2 Fick's equation

During segregation in a single crystal, atoms move to the surface via diffusion. Therefore, one can use Fick's second law [8] to describe the kinetics of segregation. Fick law states that the change in concentration with time is equal to the diffusion rate multiplied by the second order derivative of the concentration to the spatial plane position under consideration.

Mathematically it is expressed as

$$\frac{\partial C}{\partial t} = D\frac{\partial^2 C}{\partial x^2} \tag{2.1}$$

where C is the concentration, D is the diffusion coefficient, x is the distance and t is time. Initially the surface concentration of diluted species is assumed to be same as the bulk. Thus

$$C = C_B \text{ for } x > 0 \text{ and } t = 0 \tag{2.2}$$

where C_B is the bulk concentration.

If it is to be assumed that the segregating atoms do not interact with the atoms that are already on the surface, then the rate of segregation is independent of the surface concentration and the following boundary conditions may be used:

$$C = 0 \text{ at } x = 0 \text{ for all } t \geq 0 \tag{2.3}$$

A schematical representation of the concentration profile at progressing times can be seen in figure 2.2. Solving equation 2.1 [16] using the boundary conditions 2.2 and 2.3 gives

$$C_S = C_B \left[1 + \frac{2}{d}\left(\frac{Dt}{\pi}\right)^{\frac{1}{2}} \right] \tag{2.4}$$

where C_S is the surface concentration, d is the thickness of the segregated layer, which is usually the distance between two atomic layers. It is clear that C_S is dependent on the square root of t. The weaknesses of the model can be clearly seen in that as $t \to \infty$ that $C_S \to \infty$. It was also assumed that the atoms on the surface do not interact with each other, though in reality that is not the case. It should also be noted that the model is only accurate for small values of t, in other words the initial segregation of the species, as can be seen in figure 2.3.
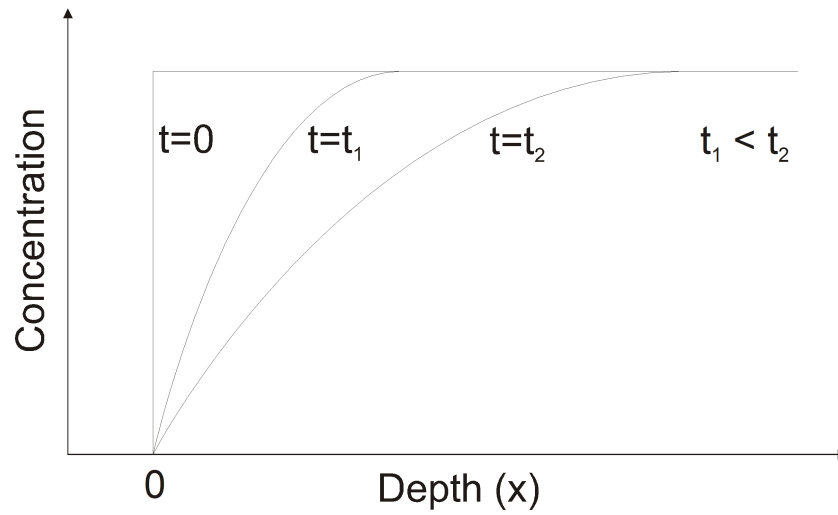
Figure 2.2: The concentration profiles at different times with the initial values and boundary conditions imposed.
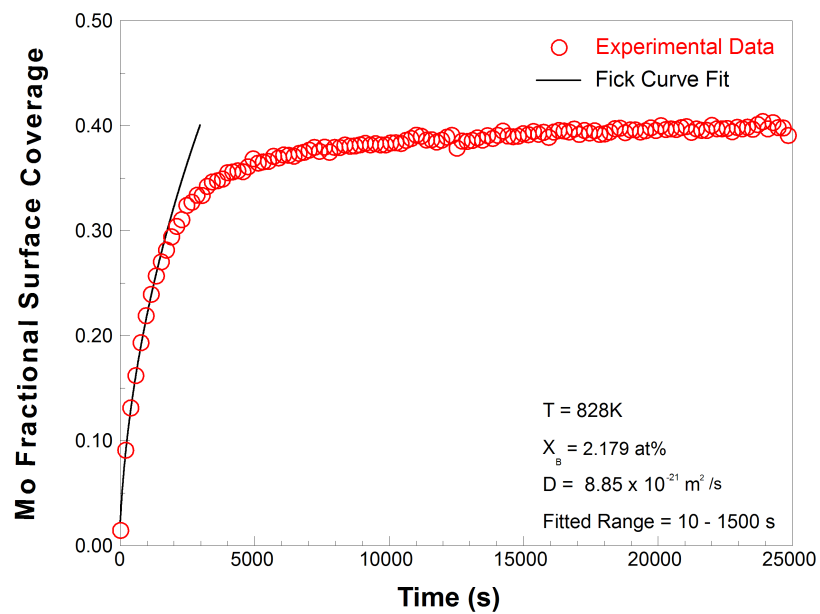

Figure 2.3: An example of experimental data fitted using Fick's equation (2.4).

In equation 2.4 the effect of sputtering has not been considered. If the sample is sputtered at high temperatures, segregation and sputtering take place simultaneously and the bulk concentration will change. This means that the initial conditions as set forth in equation 2.2 are not satisfied any more. To correct for sputtering the following equation can be derived:

$$C_S = C_S^0 + C_B \left[1 + \frac{2}{d} \left(\frac{D(t + t_0')}{\pi} \right)^{\frac{1}{2}} \right] - C_B \left[\frac{2}{d} \left(\frac{Dt_0'}{\pi} \right)^{\frac{1}{2}} \right] \tag{2.5}$$

where C_S^0 is the surface concentration after sputtering and t_0' is the sputtering time. Equation 2.5 can only be applied where the bulk concentration is low [17].

2.3 The Modified Darken Approach

Most other theories, such as the Fick equation, consider the concentration gradient to be the driving force behind segregation. However, this is contradictory to physical reality, since the diffusion of atoms takes place from a low concentration in the bulk to a high concentration on the surface. Segregation takes place because the total energy of the system is not in a minimized state when the surface and bulk have the same concentration values. The total energy δE is minimized [18] when

$$(\delta E)_{S,V,n_i} = \sum_{\nu=1}^{p} \delta E^\nu \geq 0 \tag{2.6}$$

where δE^ν is given by

$$\delta E^\nu = T^\nu \delta S - P^\nu \delta V^\nu + \delta G^\nu \tag{2.7}$$

where T^ν is the temperature, S is the entropy, P^ν is the pressure, V^ν is the volume of phase ν and G is the Gibbs free energy. If the temperature and pressure are the same for all phases, then equation 2.6 reduces to

$$(\delta E^\nu)_{n_i} = (\delta G)_{n_i} \geq 0 \tag{2.8}$$

In other words, only the Gibbs free energy needs to be considered, which can be expressed in terms of the chemical potentials of the various constituents as

$$G^\nu = \sum_{i=1}^{m} n_i^\nu \mu_i^\nu \tag{2.9}$$

where n_i^ν is the number of moles of species i and μ_i^ν is the chemical potential of species i in phase ν. The segregation energy ΔG is now defined as the difference between the initial Gibbs free energy before segregation (G) and the Gibbs free energy when equilibrium is reached (G^0):

$$\Delta G = G - G^0 \tag{2.10}$$

Since the Gibbs free energy at equilibrium is lower than the value before segregation takes place, it follows that ΔG must be negative for segregation to take place. A positive ΔG value, implies the desegregation of a species (a topic that falls outside the scope of this study).

Using the previous equations and definitions, the modified Darken set of differential equations can now be derived. Darken [19] postulated that the flux of species i through a plane at $x = b$ is given by

$$J_i = -M_i C_i^{(b)} \left(\frac{\partial \mu_i}{\partial x} \right)_{x=b} \tag{2.11}$$

where $C_i^{(b)}$ is the concentration of species i in the plane, μ_i is the chemical potential and M_i is the mobility of the species. It is clear that Darken's equation is similar to that of Fick's, but that the chemical potential gradient has replaced the concentration gradient as the driving force. To apply the Darken equation to crystals, a crystal that is divided into $N + 1$ discrete layers of thickness d each, as shown schematically in figure 2.4, is considered. The flux of species i from layer $j + 1$ to layer j is then given by [16]

$$J_i^{j+1,j} = M_i C_i^{j+1} \frac{\Delta \mu_i^{j+1,j}}{d} \tag{2.12}$$

where

- M_i is the mobility of the atoms of species i and it is related to the diffusion coefficient D by $D = MRT$, but only in the case of highly diluted or ideal solutions.

- C_i^{j+1} is the amount of atoms/m^3 of species i in layer $j+1$

- $\Delta\mu_i^{j+1,j}$ is the difference in chemical potential of species i in layer $j+1$ and j, defined as

$$\Delta\mu_i^{(j+1,j)} = (\mu_i^{(j+1)} - \mu_i^{(j)}) - (\mu_m^{(j+1)} - \mu_m^{(j)}) \qquad (2.13)$$

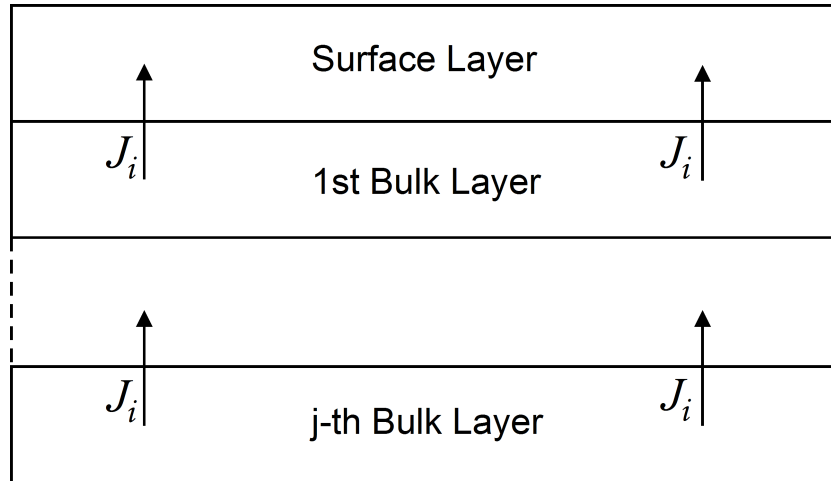for $i = 1 \ldots m$ in an alloy of m components, where m is the solvent.

Figure 2.4: A schematical representation of the flux J_i of species i to the surface of a crystal.

The rate at which the concentration of species i in layer j increases or decreases is given by the net flux into or out of layer j divided by d

$$\frac{\partial C_i^{(j)}}{\partial t} = \frac{J_i^{(j+1,j)} - J_i^{(j,j-1)}}{d} \qquad (2.14)$$

By substituting equation 2.12, the following system of equations is derived [20]

$$
\begin{aligned}
\frac{\partial X_i^S}{\partial t} &= \left(\frac{M_i^{B_1 \to S} X_i^{B_1}}{d^2} \Delta \mu_i^{B_1,S} \right) \\
\frac{\partial X_i^{B_1}}{\partial t} &= \left(\frac{M_i^B X_i^{B_2}}{d^2} \Delta \mu_i^{B_2,B_1} - \frac{M_i^{B_1 \to S} X_i^{B_1}}{d^2} \Delta \mu_i^{B_1,S} \right) \\
&\vdots \\
\frac{\partial X_i^j}{\partial t} &= \left(\frac{M_i^B X_i^{j+1}}{d^2} \Delta \mu_i^{(j+1,j)} - \frac{M_i^B X_i^j}{d^2} \Delta \mu_i^{(j,j-1)} \right) \\
&\vdots
\end{aligned}
$$

(2.15)

where X_i^j is the fractional concentration of species i in layer j.

This system of differential equations can be solved numerically, by using the variable step size Gear method [21] for example.

2.3.1   Equilibrium

As stated earlier, equilibrium is reached when δE is minimized or when there is no change in the concentrations of all species in all layers within a crystal. This can be expressed mathematically as [16]

$$
\frac{\partial X_i^j}{\partial t} = 0 \quad \text{for } i = 1, 2 \text{ and } j = 1, 2, ..., N
$$

(2.16)

Referring to equation 2.15, this means that in the case of a ternary system

$$
\mu_1^\phi - \mu_1^B - \mu_3^\phi + \mu_3^B = 0
$$

(2.17)

$$
\mu_2^\phi - \mu_2^B - \mu_3^\phi + \mu_3^B = 0
$$

(2.18)

where ϕ denotes the surface layer and B the bulk.

From these conditions the following set of equations can be derived [22]

$$X_1^\phi = \frac{X_1^B \exp\left(\frac{\Delta G_1}{RT}\right)}{1 - X_1^B + X_1^B \exp\left(\frac{\Delta G_1}{RT}\right) - X_2^B + X_2^B \exp\left(\frac{\Delta G_2}{RT}\right)} \tag{2.19}$$

$$X_2^\phi = \frac{X_2^B \exp\left(\frac{\Delta G_2}{RT}\right)}{1 - X_2^B + X_2^B \exp\left(\frac{\Delta G_2}{RT}\right) - X_1^B + X_1^B \exp\left(\frac{\Delta G_1}{RT}\right)} \tag{2.20}$$

where

$$\Delta G_1 = \Delta G_1^0 + 2\Omega_{1,3}\left(X_1^\phi - X_1^B\right) + \Omega'\left(X_2^B - X_2^\phi\right)$$
$$\Delta G_2 = \Delta G_2^0 + 2\Omega_{2,3}\left(X_2^\phi - X_2^B\right) + \Omega'\left(X_1^B - X_1^\phi\right) \tag{2.21}$$

and

$$\Omega' = \Omega_{1,2} - \Omega_{1,3} - \Omega_{2,3} \tag{2.22}$$

where ΔG_i is the segregation energy of species i and $\Omega_{i,j}$ as the interaction coefficient between species i and j.

2.3.2 The special case of a binary bulk and a ternary surface

The Fe-3.5wt%Mo(100) sample investigated in this study was exposed to a nitrogen ambient to promote the segregation of molybdenum. All three elements (i.e. Fe, Mo and N) are found on the surface, but the bulk does not contain nitrogen. Thus, the bulk is a binary system and the surface is a ternary system. It has been shown by Viljoen *et al* [23] that at high temperatures the adsorption of nitrogen becomes the limiting factor on the segregation rate of molybdenum and that the molybdenum and nitrogen are then in equilibrium at the surface.

From this premise it is assumed that ΔG_{Mo} is an unknown function of X_N^ϕ, $\Delta G'(N)_{Mo}$ and equation 2.19 therefore becomes

$$X_{Mo}^\phi = \frac{X_{Mo}^B \exp\left(\frac{\Delta G'(N)_{Mo}}{RT}\right)}{1 - X_{Mo}^B + X_{Mo}^B \exp\left(\frac{\Delta G'(N)_{Mo}}{RT}\right) - X_N^B + X_N^B \exp\left(\frac{\Delta G_N}{RT}\right)} \qquad (2.23)$$

However, the bulk concentration of N is zero for the binary system. By substituting $X_N^B=0$ in equation 2.23, it becomes

$$X_{Mo}^\phi = \frac{X_{Mo}^B \exp\left(\frac{\Delta G'(N)_{Mo}}{RT}\right)}{1 - X_{Mo}^B + X_{Mo}^B \exp\left(\frac{\Delta G'(N)_{Mo}}{RT}\right)} \qquad (2.24)$$

Rearranging the equation and collecting terms, $\Delta G'(N)_{Mo}$ becomes

$$\Delta G'(N)_{Mo} = -RT \ln\left(\frac{X_{Mo}^\phi(1 - X_{Mo}^B)}{X_{Mo}^B(1 - X_{Mo}^\phi)}\right) \qquad (2.25)$$

X_{Mo}^B is a known value and X_{Mo}^ϕ is measured, allowing $\Delta G'(N)_{Mo}$ to be calculated. By plotting the values against X_N^ϕ, an expression in terms of X_N^ϕ can be derived by doing a polynomial fit, as will be shown in Chapter 4.

2.3.3 Simulations

The influences of the various parameters discussed are better understood via a few simulations. These simulations were done by the author using the *Darken 3C* software package [15]. A more detailed discussion of these parameters can be found in [16]. Firstly, default values are chosen for both segregating species. These values are chosen to be the same for both species and can be seen in table 2.1. From these values, a reference segregation profile is generated as seen in figure 2.5. The two curves lie on each other as expected. The parameters are then individually adjusted (temperature excluded) to see the effect it has on the kinetics and equilibrium state. These adjustments can be seen in table 2.2. Some parameters are common to both species and only one of them (species 1) needs to be changed in order to observe its effect.

Table 2.1: The default parameters chosen for the two segregating species of a ternary system. D is the diffusion coefficient, ΔG is the segregation energy, X_B is the bulk concentration and Ω is the interaction coefficient between the relevant species.

Species	D (m^2/s)	ΔG (kJ/mol)	X_B (at%)	$\Omega_{x,3}$ (kJ/mol)	$\Omega_{1,2}$ (kJ/mol)	Temp. (K)
1	5x10^{-21}	-50	1	0	0	800
2	5x10^{-21}	-50	1	0		

Table 2.2: The adjustments made to the default parameters in table 2.1. Note that "+" and "-" indicate an increase or decrease of the absolute values respectively.

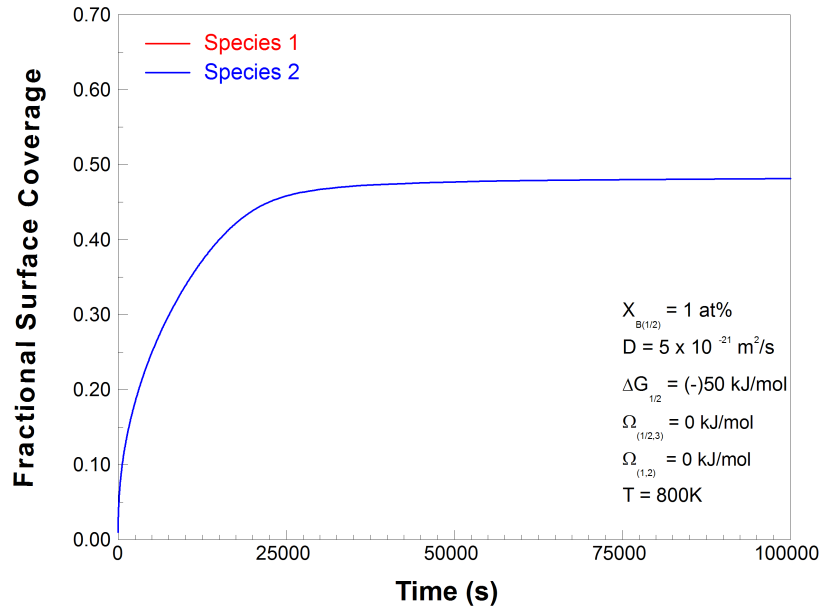| Parameter	Value	Figure
ΔG_1 (kJ/mol)	+2; +4; +6	2.6
	-2; -4; -6	2.7
$X_{B(1)}$ (at%)	0.75; 0.5; 0.25	2.8
D_1 (m^2/s)	x2; x4; x6	2.9
	/2; /4; /6	2.10
$\Omega_{1,3}$ (kJ/mol)	+2; +4; +6	2.11
	-2; -4; -6	2.12
$\Omega_{1,2}$ (kJ/mol)	+20; +30; +40; +60	2.13
	-5; -15; -30	2.14

Figure 2.5: The reference ternary system segregation profile generated using the default parameters in table 2.1. (Note that the two curves lie on each other and are therefore indistinguishable.)

Segregation energy ΔG:

The first parameter considered is the segregation energy, ΔG. As can be seen in figure 2.6, both species seem unaffected during the initial segregation up to 20000 seconds because they have the same diffusion coefficient and the influence of the segregation energy has not come into effect yet. Thereafter the two curves start deviating from each other as the two species start experiencing site competition. Species 1, having the higher segregation energy of the two species, reaches a higher equilibrium concentration. In the case of a lower segregation energy the opposite effect is observed as seen in figure 2.7. Thus, the primary function of segregation energy is to determine the segregation rate and the equilibrium concentration of a species, but it is not an exclusive role, since the bulk concentration also effects the equilibrium concentration as seen in figure 2.8. In comparison with the reference curve, the curves have same shape and still reach equilibrium at the same time. Furthermore, it is interesting to note that the sum of the equilibrium concentrations of the two species is constant, since the sum of the their segregation energies are the same throughout.
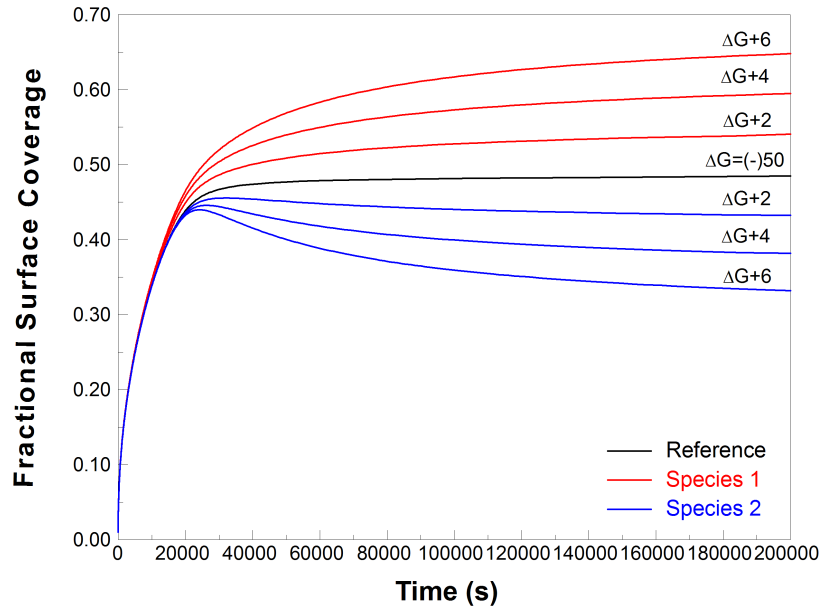
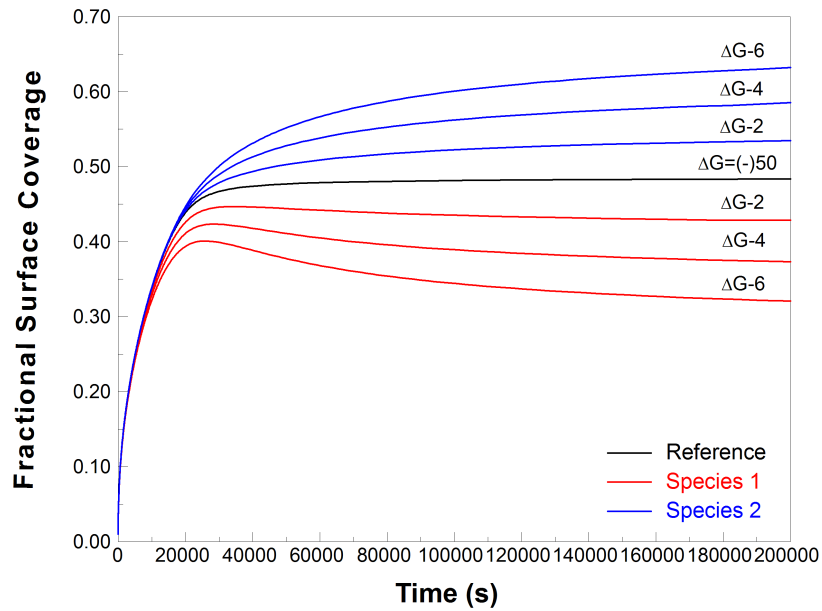Figure 2.6: The effect of a higher segregation energy on the segregation profile.

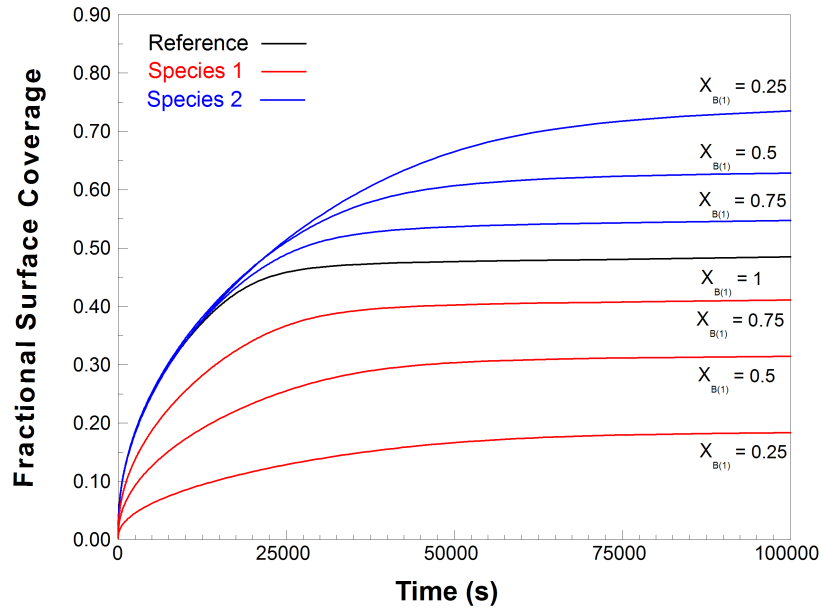Figure 2.7: The effect of a lower segregation energy on the segregation profile.

Figure 2.8: The effect of a lower bulk concentration on the segregation profile.

Diffusion coefficient D:

As can be seen in figure 2.9, an increase in the diffusion coefficient yields a steeper slope in the initial segregation of species 1. During this period the system behaves in a binary fashion in that species 2 seems unaffected by species 1. Thereafter the two species start experiencing site competition again and with both species having the same segregation energy, the concentration of species 1 starts decreasing while the concentration of species 2 is still increasing and eventually they will both reach the same concentration. Again the opposite behaviour is observed for a lower diffusion coefficient as can be seen in figure 2.10.

Interaction coefficient $\Omega_{(1,3)}$:

Finally, we consider the effects of the interaction coefficients. As can be seen in figure 2.11 a positive interaction coefficient between species 1 and the bulk $\Omega_{(1,3)}$ causes a higher equilibrium concentration for species 1. If compared to figure 2.6 it is clear that this curve is very similar to that of a segregation energy of equivalent value. Referring to figures 2.12 and 2.7, the same conclusion can be made for a negative value. Because the graphs are nearly indistinguishable it is common practice to set the interaction coefficient between segregating species and the bulk to zero. This has the positive advantage of making experimental curve fits easier, but one should keep in mind that $\Omega_{(1,3)}$ is not always zero.
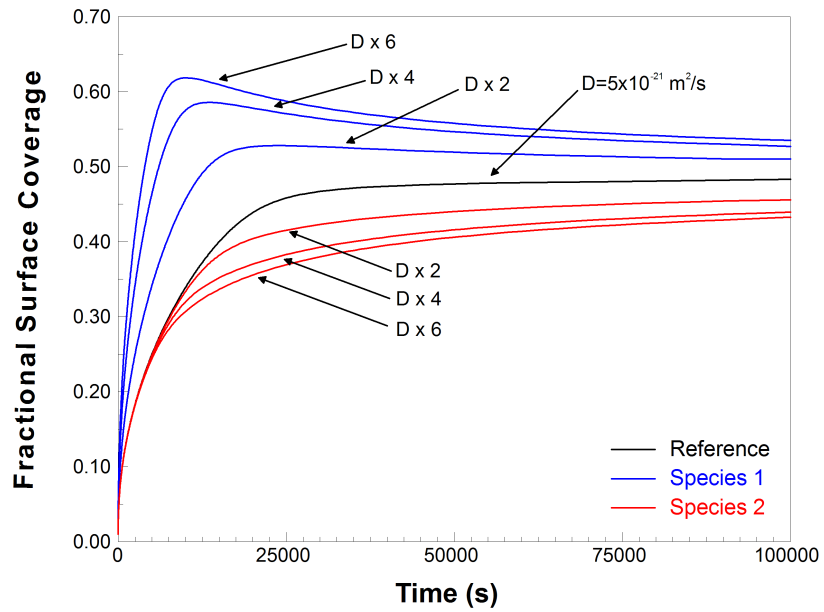
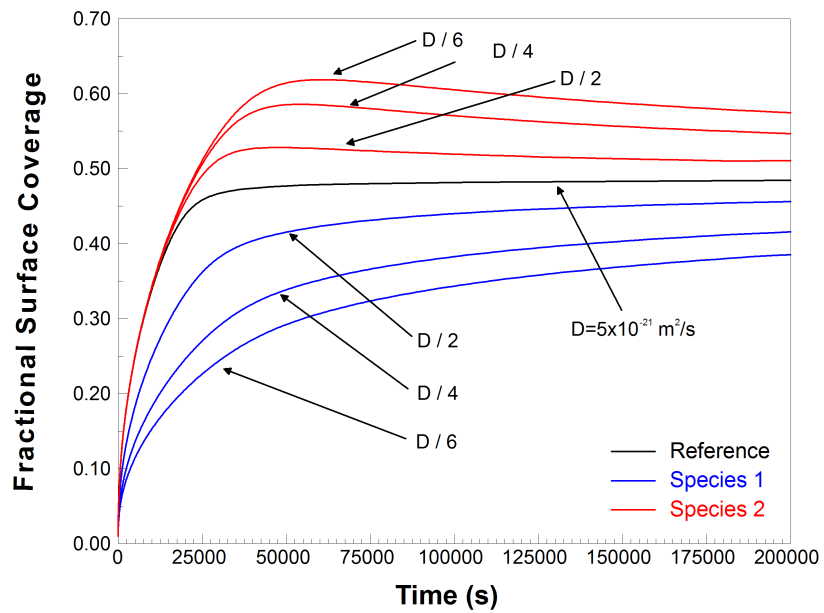Figure 2.9: The effect of a higher diffusion coefficient on the segregation profile.

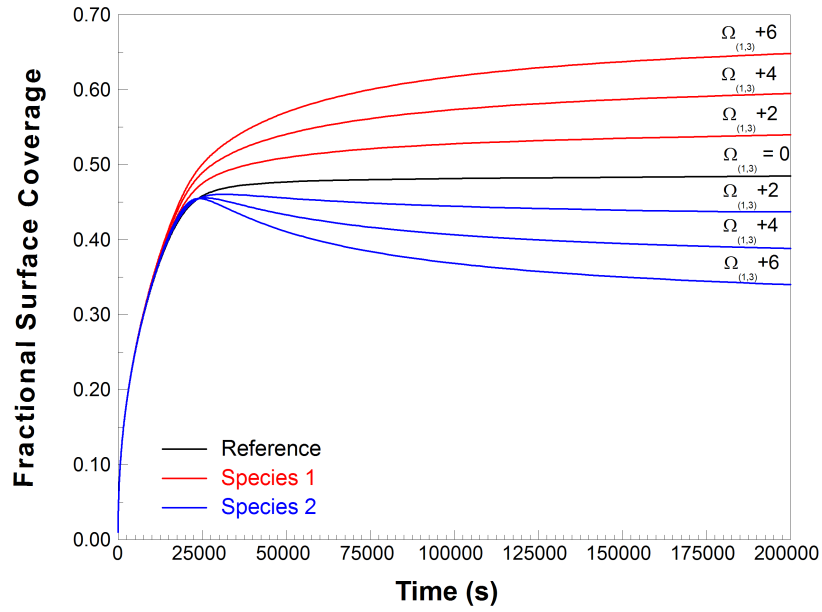Figure 2.10: The effect of a lower diffusion coefficient on the segregation profile.

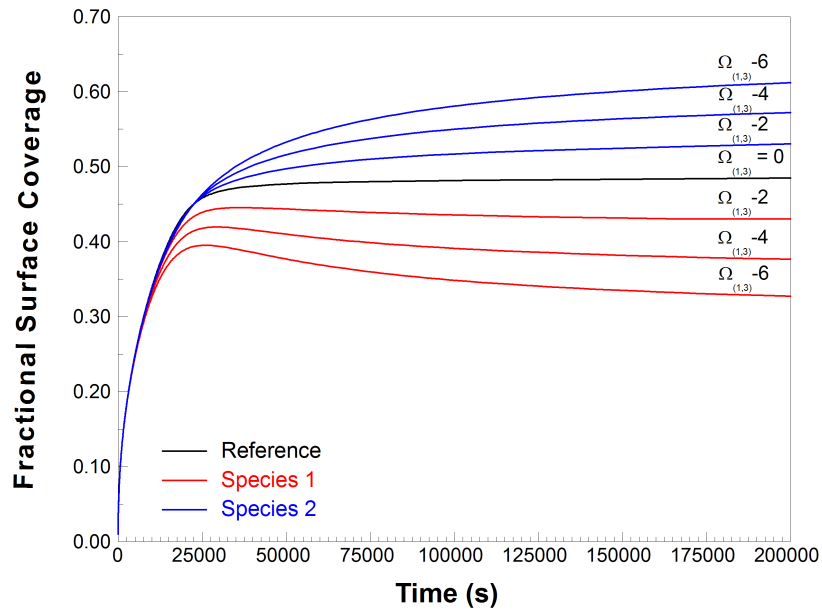Figure 2.11: The effect of a positive interaction coefficient between a segregating species and the bulk.

Figure 2.12: The effect of a negative interaction coefficient between a segregating species and the bulk.

Interaction coefficient $\Omega_{(1,2)}$:

Therefore, the only interaction coefficient that is of importance, is that between the segregating species themselves, $\Omega_{(1,2)}$. In the case of co-segregating species, it has a non-zero value by definition. From figure 2.13 it is observed that a positive value has a repulsive effect between the two species. Although it seems that the two species will reach equilibrium together, they start to deviate earlier with increasing values of $\Omega_{(1,2)}$. All the other parameters are the same for both species though, so there is no reason for any preference to exist and it is observed that the two species swap places at 60 kJ/mol. It is concluded that a repulsive interaction coefficient creates an unstable state and that small changes in the surface concentration can cause the desegregation of a species at another's cost. For negative values of $\Omega_{(1,2)}$, the opposite behaviour is observed (figure 2.14). The two species are attracted to each other and they segregate together (i.e. the graphs lie on each other), reaching equilibrium earlier with increasing values of $\Omega_{(1,2)}$.
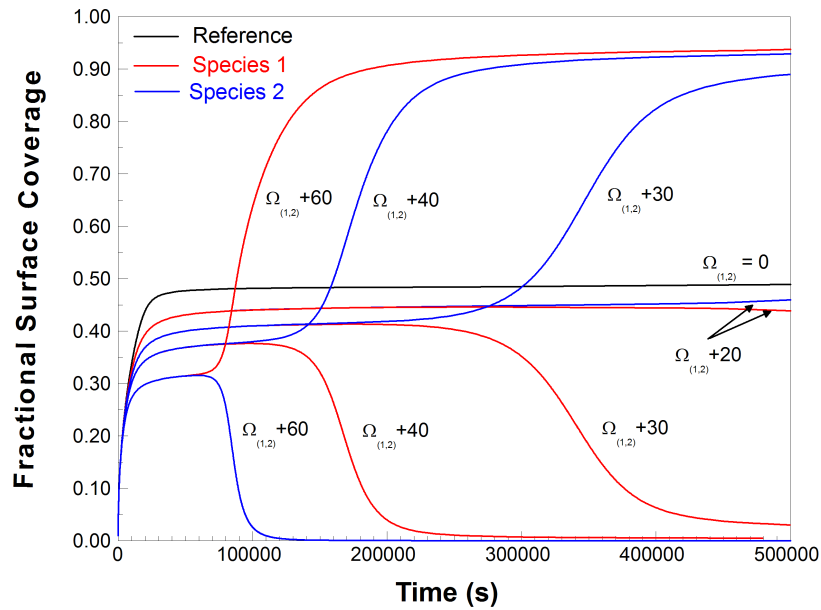

Figure 2.13: The effect of a positive interaction coefficient between the two segregating species.
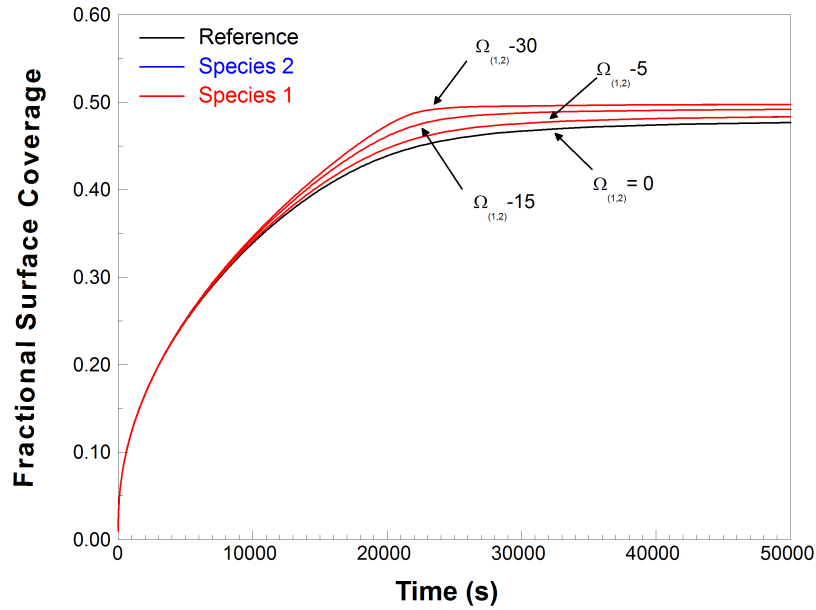
Figure 2.14: The effect of a negative interaction coefficient between the two segregating species.

2.4   Summary

In this chapter, the theory behind segregation, as applied to this study, was discussed. There are other theories that can also be applied, but Fick's equation was chosen for its ease of use and effectiveness at determining the diffusion coefficients of segregating species. It was shown that Fick's equation, which considers the concentration gradient $\partial C/\partial x$ as the driving force behind segregation, has limitations and that it was used together with the modified Darken approach, which considers the chemical potential gradient $\partial \mu/\partial x$ as the driving force. Using the Darken approach, additional parameters can also be acquired. The influences of these parameters on the segregation kinetics were illustrated via simulations. It was shown that the segregation energy ΔG and the bulk concentration X_B determine the equilibrium concentrations. Furthermore, is was found that the interaction coefficient between the segregating species and the bulk $\Omega_{1/2,3}$ can be discarded, but that the interaction coefficient between the species $\Omega_{1,2}$ has a tremendous effect on the kinetics and is vital in the case of co-segregation. In the next chapter, the experimental setup used to acquire the segregation profiles will be discussed in detail.

Chapter 3

Experimental Setup

3.1 Introduction

Previous segregation studies have been done on the Fe-3.5wt%Mo-N(100) ternary system by Uebing *et al* [9][10][11]. Where the aforementioned studies have focused on equilibrium segregation, the purpose of this study is to determine the kinetic segregation coefficients of the Fe-3.5wt%Mo-N(100) system. Two single crystals were chosen for this purpose, one which is a binary system and the other, a ternary system. The binary system is a Fe-3.5wt%Mo(100) single crystal which is exposed to a nitrogen ambient at $5x10^{-7}$ Torr during measurement. The nitrogen is adsorbed on the surface, allowing the Mo to segregate to the surface. In effect the surface is a ternary system. The ternary system is a Fe-3.5wt%-Mo-N(100) single crystal. Since the parameters that need to be determined for the binary system are less (3 as opposed to 7), they are easily determined by comparison. Using the values determined for the binary system as estimates, the coefficients for the ternary system may be determined.

The surface analysis method chosen for determining the surface concentration of the elements, was Auger Electron Spectroscopy (AES)[24]. Other surface sensitive techniques may be considered, such as X-Ray Photoelectron Spectroscopy (XPS)[25], Ion Scattering Spectroscopy (ISS)[26] and Secondary Ion Mass Spectroscopy (SIMS)[27], for measuring the surface concentration of the segregated species. However, the advantages of AES such as quick data collection, non-destructiveness and relative ease of quantification have been discussed by Hofmann [28] and the conclusion was made that AES is the most suitable method for kinetic measurements. The principles of AES measurement are well documented [29] and therefore only the quantification and measurement system will be discussed.

Together with the AES concentration measurements, accurate surface temperature measurements are essential for segregation studies. For this study, an infrared (IR) thermometer was used to measure the surface temperature. Not only is it more accurate, it is easier to use and there is no need to spot weld a thermocouple onto the surface of a sample and thereby damaging it. To insure accurate temperature readings, the IR thermometer was calibrated against a Chromel-Alumel thermocouple on a substitute crystal. The temperature measurement unit which reads the voltage over the thermocouple was calibrated using a calibrated power supply and multimeter.

At the end of this chapter a summary is given of the analysis procedure.

3.2 Sample preparation

The crystals used in this study were acquired from the Max-Plank-Institut für Eisenforschung. They were made using the Bridgman method [30] and contain 96.5 wt% Fe and 3.5 wt% Mo. The one crystal contains 10 wt.ppm N, determined via atomic absorpsion. The samples were spark-eroded to 1.5 mm thickness and $\pm$ 1 deg of the desired crystallographic orientation. The sample were cut to 5x5x1.5 mm pieces. Prior to analysis, the crystals were mechanically polished to 0.05 μm using alumina paste until a mirror-like finish has been obtained.

3.3 AES

3.3.1 AES System

A schematical representation of the AES system can be seen in figure 3.1. All measurements were done by computer using the VisiScan software [31]. The personal computer has a PC-66 Digital-to-Analog (D/A) card, and a PC-30 Analog-to-Digital (A/D) card. The PC-66 controls various output functions of the system, such as the required scanning energy, required temperature and the IR thermometer parameters. The PC-30 card functions as a input device that collects data from the system, such as the AES signal and temperature.

The system consists of the following components:

- Perkin Elmer 20-320A Electron Gun. It has a variable primary electron energy E_P of 0 - 10 keV. The primary electron beam energy was set at 3 keV for all measurements. The filament current was set at 2.7 A and the emission current used was between 1 mA and 1.5 mA. A beam current of 10 to 15 μA was used.

- Perkin Elmer 20-070 Scanning Control Unit. This unit controls the XY position of the electron beam on the surface of the sample and may be used to raster the electron beam over the surface. Since segregation measurements are done at a point, the XY position was fixed at 0,0.

- Perkin Elmer 15-110B Cylindrical Mirror Analyzer (CMA). The aperture was set to the medium size, resulting in a good balance between resolution and sensitivity.

- Perkin Elmer 11-500A Auger System Control. This unit controls the scanning energy by changing the voltage on the outer cylinder of the CMA. It was operated in the external mode, allowing the PC to control the value.

- PHI 415B 0 - 3000 V High Voltage Supply with Electron Multiplier. A multiplier voltage of 1950 V was used for analysis and the elastic peak was optimized at 1250 V.

- PHI 122 Lock-in Amplifier. It has a variable time constant of 0 - 30 seconds and a sensitivity of 0.1 - 50 mV. Since the AES signal is averaged by the PC, the time constant was set to zero. A sensitivity of 1 mV and modulation amplitude of 4 eV was used.

- PHI 04-177 Ion gun. This unit has variable primary energy of 0.5 - 4 keV. An emission current of 25 mA, as recommended by the manufacturer, was used. The rastering size is adjustable between 0x0 mm and 10x10 mm. A value of 5x5 mm was used to sputter clean the sample prior to analysis.

- Temperature Control Unit. This unit regulates the temperature of the sample. It may be used to increase the temperature linearly or it can maintain a constant temperature. The constant temperature function was used for this study.

- 240 l/s Ion Pump. With this unit a typical base pressure of $< 10^{-8}$ Torr can be achieved after the system has been baked out.

For measuring the surface concentration against time, the multiplexer function of the VisiScan software was used. In this mode the voltage on the plates of the CMA are controlled by the PC-66 card. The Auger-signal from the Lock-in amplifier is
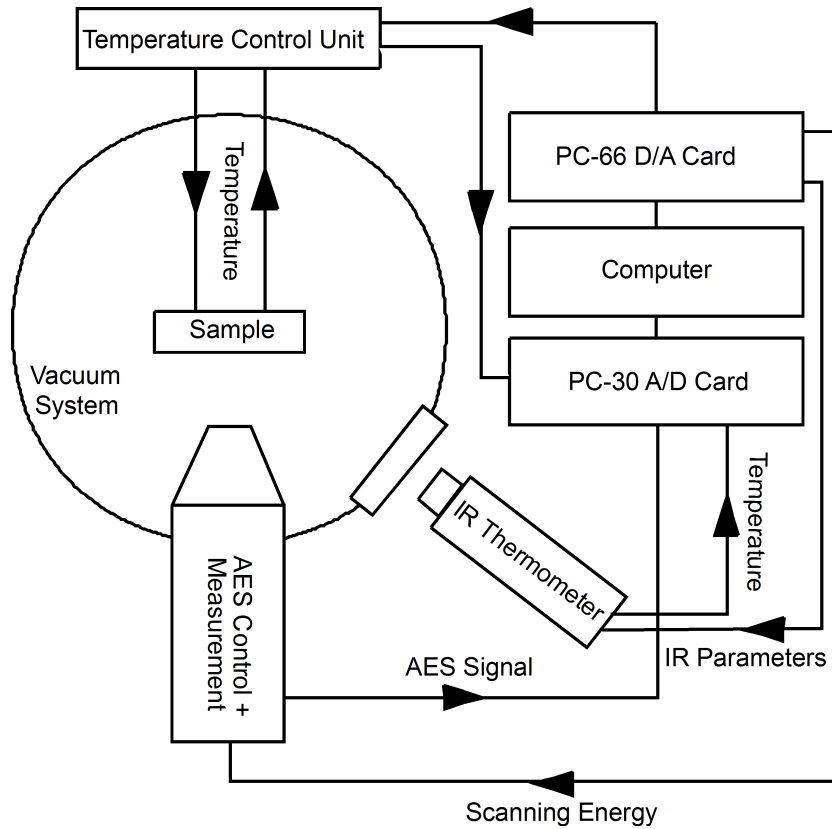
Figure 3.1: Schematical representation of AES system. The arrows indicate the direction of data/signal flow.

read through the PC-30 card. To minimize the noise, multiple readings are taken and averaged. The maximum frequency at which the PC-30 card can record analog signals is 330 Hz. Thus, the shortest time interval between readings is 3 ms. It follows that the time spend on a channel is

$$time\,per\,channel = \frac{upper\,boundary - lower\,boundary}{scanrate * number\,of\,channels}$$

The equation above imposes a limitation on the time taken to scan the entire Auger spectrum. Since the surface segregation kinetics are quite rapid, it would be impractical to scan the entire Auger spectrum during this type of measurement. Thus the multiplexer function of the software package is used to monitor only the elemental peaks of interest.

3.3.2 AES Quantification

Suppose a electron beam with primary current I_0 and primary energy E_p falls on a matrix M and generates Auger electrons which are analyzed with a spectrometer positioned at an angle θ with respect to the sample. The transmission efficiency of the spectrometer is $T(E_A)$ and the transmission efficiency of the electron multiplier is $D(E_A)$. The total Auger current from element A in matrix M is then given by [32]

$$I_A = I_0\sigma_A(E_p)[1 + r_A^M(E_A,\alpha)]T(E_A)D(E_A)*$$
$$\int_0^\infty N_A(z)\exp[-z/\lambda_A^M(E_A)\cos\theta]dz \quad (3.1)$$

where

- the matrix is assumed to be a continuum medium,

- the Auger probability cross-section of element A is σ_A,

- the backscattering factor $r_A^M(E_A,\alpha)$ is dependent on the matrix M and the binding energy of the electrons in the Auger transition is given by E_A,

- $N_A(z)$ is element A's concentration at a depth z from the surface,

- $\lambda_M(E_A)$ is the inelastic free path of an Auger-electron of element A in matrix M.

However a crystal is a discreet medium with well defined atomic layers and thus the total Auger-current would rather be described by

$$I_A = I_0\sigma_A(E_P)[1 + r_A^M(E_A,\alpha)]T(E_A)D(E_A)*$$
$$\sum_{n=0}^{n=\infty} N_A(nd)\exp[-nd/\lambda_A^M(E_A)\cos\theta] \quad (3.2)$$

where d is the distance between atomic layers.

The most important difference between the discreet and continuum models is the way electrons from the first layer are observed [33]. Thus, the calculated surface concentration is different depending on which model is used. Unfortunately, the inelastic mean free path of the Auger-electrons and the backscattering factors have been calculated for a continuum medium [34][35]. To overcome this difficulty, the number of unknowns in the continuum model (3.1) are reduced by comparing the

Auger current from element A in matrix M with the total Auger current I_A^∞ from a pure standard of element A. Thus,

$$\frac{I_A^M}{I_A^\infty} = \frac{[1 + r_A^M(E_A, \alpha)] \int_0^\infty N_A(z) \exp[-z/\lambda_A^M(E_A) \cos\theta] dz}{[1 + r_A^\infty(E_A, \alpha)] \int_0^\infty N_A(z) \exp[-z/\lambda_A^\infty(E_A) \cos\theta] dz} \tag{3.3}$$

In the case of monolayer segregation where the surface layer composition is different from the bulk, the contribution to the Auger signal from element A from the different layers is given by,

$$
\begin{aligned}
&\int_0^\infty N_A(z) \exp\left(\frac{-z}{\lambda_A^M \cos\theta}\right) dz \\
=\; & \int_0^d N_A(z) \exp\left(\frac{-z}{\lambda_A^M \cos\theta}\right) dz + \int_d^\infty N_A(z) \exp\left(\frac{-z}{\lambda_A^M \cos\theta}\right) dz \\
=\; & \frac{X_A^S}{a_M^3 d} \int_0^d \exp\left(\frac{-z}{\lambda_A^M \cos\theta}\right) dz + \frac{X_A^B}{a_M^3 d} \int_d^\infty \exp\left(\frac{-z}{\lambda_A^M \cos\theta}\right) dz \\
=\; & \frac{\lambda_A^M \cos\theta}{a_M^3} \left[X_A^S - X_A^S \exp\left(-\frac{d}{\lambda_A^M \cos\theta}\right) + X_A^B \exp\left(-\frac{d}{\lambda_A^M \cos\theta}\right) \right] \tag{3.4}
\end{aligned}
$$

where X_A^S is the fractional concentration of element A in the surface layer, X_A^B is the fractional concentration of element A in the bulk, a_M is the atomic size of the matrix M and d is the interlayer distance.

For a pure single element standard it follows that,

$$\int_0^\infty N_A(z) \exp\left(\frac{-z}{\lambda_A^\infty \cos\theta}\right) dz = \frac{\lambda_A^\infty \cos\theta}{a_A^3} \tag{3.5}$$

where a_A^3 is the atomic size of element A. If equations 3.5 and 3.4 are substituted in equation 3.3, the total Auger current of the pure element A can be calculated in terms of the Auger current of element B. This relationship is given by

$$
\begin{aligned}
\frac{I_A^M}{I_B^M} = {} & \frac{I_A^\infty [1 + r_A^M(E_A, \alpha)][1 + r_B^\infty(E_B, \alpha)] \lambda_A^M \lambda_B^\infty a_A^3}{I_B^\infty [1 + r_B^M(E_B, \alpha)][1 + r_A^\infty(E_A, \alpha)] \lambda_B^M \lambda_A^\infty a_B^3} \\
& \frac{X_A^S - X_A^S \exp(-d/\lambda_A^M \cos\theta) + X_A^B \exp(-d/\lambda_A^M \cos\theta)}{X_B^S - X_B^S \exp(-d/\lambda_B^M \cos\theta) + X_B^B \exp(-d/\lambda_B^M \cos\theta)}
\end{aligned}
\tag{3.6}
$$

where all the symbols for element B have the same meaning as defined before.

Now X_A^S can be solved from the above equation

$$X_A^S = \frac{I_A^M}{I_B^M \Omega} \left[X_B^S \frac{1 - \exp(-d/\lambda_B^M \cos\theta)}{1 - \exp(-d/\lambda_A^M \cos\theta)} + X_B^B \frac{\exp(-d/\lambda_B^M \cos\theta)}{1 - \exp(-d/\lambda_A^M \cos\theta)} \right]$$
$$- X_A^B \frac{\exp(-d/\lambda_A^M \cos\theta)}{1 - \exp(-d/\lambda_A^M \cos\theta)} \quad (3.7)$$

where

$$\Omega = \frac{I_A^\infty [1 + r_A^M(E_A, \alpha)][1 + r_B^\infty(E_B, \alpha)] \lambda_A^M \lambda_B^\infty a_A^3}{I_B^\infty [1 + r_B^M(E_B, \alpha)][1 + r_A^\infty(E_A, \alpha)] \lambda_B^M \lambda_A^\infty a_B^3} \quad (3.8)$$

For this study, the concentration of Mo and N in the surface layer are calculated based on the following assumptions

- The Mo concentration in the bulk is 3,5 wt% or 2,2 at%

- The N concentration in the bulk is negligible

- The total Auger current for each element is given by the Auger Peak to Peak Height (APPH) value

- The relative Auger current for a pure sample of each element is given by the relative sensitivity factor as in [36]

- The backscattering factor r can be calculated using Shimizu's equation [37]

$$r = 1 + 2.8 \left(1 - 0.9\frac{E_b}{E_p}\right) \eta \quad (3.9)$$

where E_b is the ionization energy of the Auger electrons, E_p is the primary electron energy and η is a function of the atomic number Z

$$\eta = -0.0254 + 0.016Z - 0.000186Z^2 + 8.3x10^{-7}Z^3 \quad (3.10)$$

- The escape depth λ is given by the TPP-2 equation [38]

$$\lambda = E/\{E_p^2[\beta\ln(\gamma E) - (C/E) + (D/E)^2]\} \tag{3.11}$$

  where

  1. E is the electron energy
  2. $E_p = 28.8(N_V\rho/M)^{1/2}$ is the free electron plasmon energy, with N_V the amount of valence electrons, ρ is the bulk density and M the atomic mass
  3. $\beta = 0.0216 + 0.944/E_p + 7.39x10^{-4}\rho$
  4. $\gamma = 0.191\rho$
  5. $C = 1.97 - 0.91N_V\rho/M$
  6. $D = 53.4 - 20.8N_V\rho/M$

- The inter planar distance d is given by [39]

$$d = \frac{a}{\sqrt{h^2 + k^2 + l^2}} \tag{3.12}$$

  where a is the matrix constant and hkl are the Miller-indexes of the plane. Thus, for a Fe(100) crystal it follows that $d = a = 0.2886$ nm.

3.4 Temperature Calibration

3.4.1 Thermocouple

The thermocouple used for the calibration of the IR thermometer was made by spot welding two wires, one made from chromel and one made from alumel, to a substitute Fe crystal. There exists a voltage (V) over the two wires of the thermocouple which is temperature (T) dependent. Although this relationship is almost linear, it was found that the average deviation from the true value, as given by Weast[40], was 2.07 K when linear regression was done. Since accurate temperature measurements are critical to segregation studies this value was unacceptable. A third degree polynomial function was fitted as recommended by Holman [41] and the average deviation was then found to be 0.63 K, which is smaller than the resolution of the temperature control unit, i.e. 1 K.

The equation describing the polynomial as seen in figure 3.2 is given by:

$$T = a_3 V^3 + a_2 V^2 + a_1 V + a_0 \tag{3.13}$$

where

- $a_3 = (2.09 \pm 0.19) \text{x} 10^{-3}$

- $a_2 = -0.138 \pm 0.013$

- $a_1 = 26.48 \pm 0.22$
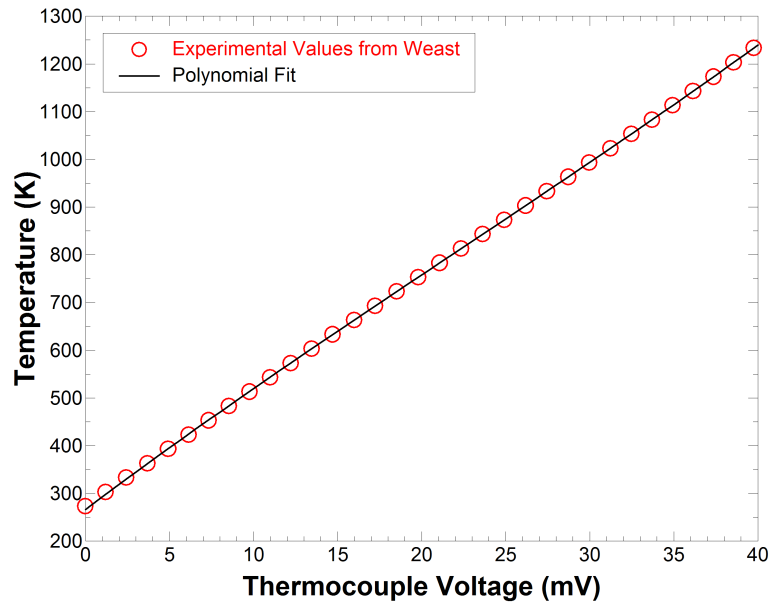
- $a_0 = 266.5$

Figure 3.2: The relationship between the voltage and temperature of a chromel-alumel thermocouple.

Before the IR thermometer could be calibrated against the substitute Fe crystal, it was insured that the PC read the voltages correctly by using a calibrated power supply and a digital multimeter. These were connected to the chromel and alumel wires that go into the Temperature Control Unit and thus simulated a thermocouple. The room temperature is already determined by the linear heating unit as a voltage which is added to the thermocouple voltage. Thus, the sum of these two voltages are then amplified and read by the computer as the output voltage.
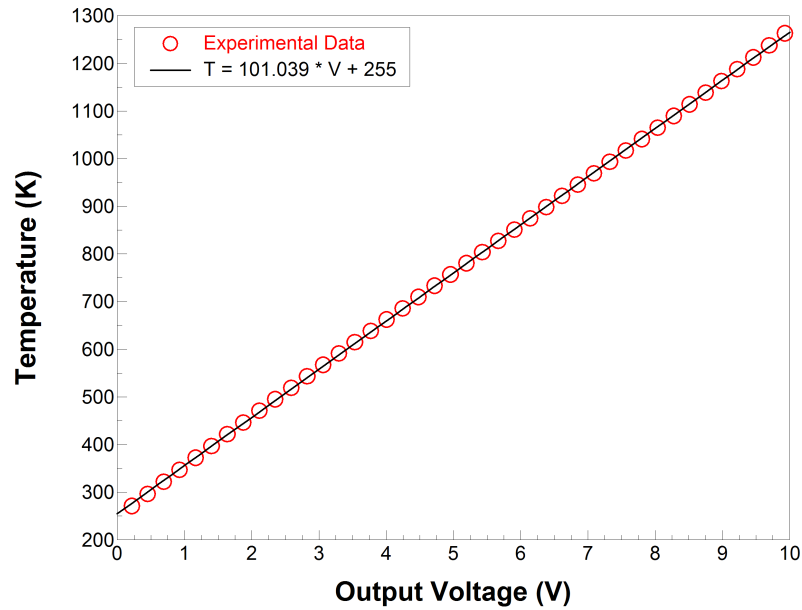
Figure 3.3: Temperature calculated from equation 3.13 versus the output voltage read by the computer.

By using equation 3.13, the temperature is calculated from the input voltage. The relationship between the temperature and output voltage is shown in figure 3.3. Linear regression was done on the data and it was found that

$$T = 101.039V + 255 \qquad (3.14)$$

with a very reasonable R^2 value of 0.999939.

Because the room temperature voltage has been added to the output voltage, the true temperature was calculated by the computer using only the slope of equation 3.14.

3.4.2 Infrared Thermometer

IR thermometers have to be calibrated against known standards as different materials have different emissions at different temperatures. So, by using a substitute Fe single crystal and a thermocouple that has been calibrated by the aforementioned procedure, the IR thermometer could be calibrated for use on the two analysis samples used in this study. It should be mentioned that the calibration can only be done in the AES system as the window might affect the observed temperature by attenuating the IR radiation. Also, to insure that the emission characteristics are
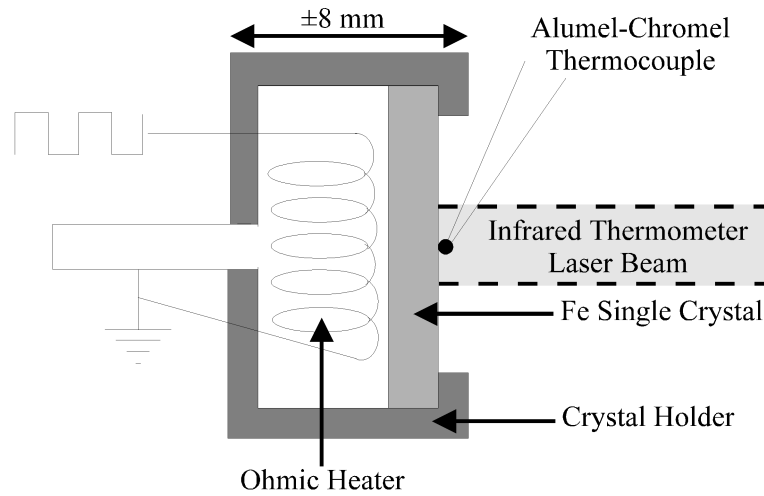
Figure 3.4: The experimental setup used to calibrate the IR thermometer.

the same for all the samples, the substitute crystal was also mechanically polished to 0.05 μm.

A thermocouple was spot welded onto the substitute before insertion into the AES system. The system was pumped down to a vacuum of $<5\text{x}10^{-9}$ Torr. A schematical representation of the calibration setup can be seen in figure 3.4. The crystal was heated linearly from 470 K to 1070 K. A heating rate of 0.1 K/s was used to insure that the temperature gradient over the crystal was negligible. The IR thermometer reading and the thermocouple reading were taken simultaneously at 3 second intervals.

The thermocouple reading or the true temperature, was plotted as a function of the IR thermometer reading as seen in figure 3.5. A second order polynomial was fitted to the experimental data and it was found that

$$T_{TC} = a_2 T_{IR}^2 + a_1 T_{IR} + a_0 \tag{3.15}$$

where

- $a_2 = (1.595 \pm 0.011)\text{x}10^{-4}$

- $a_1 = 1.1257 \pm 0.0017$

- $a_0 = -26.38135$
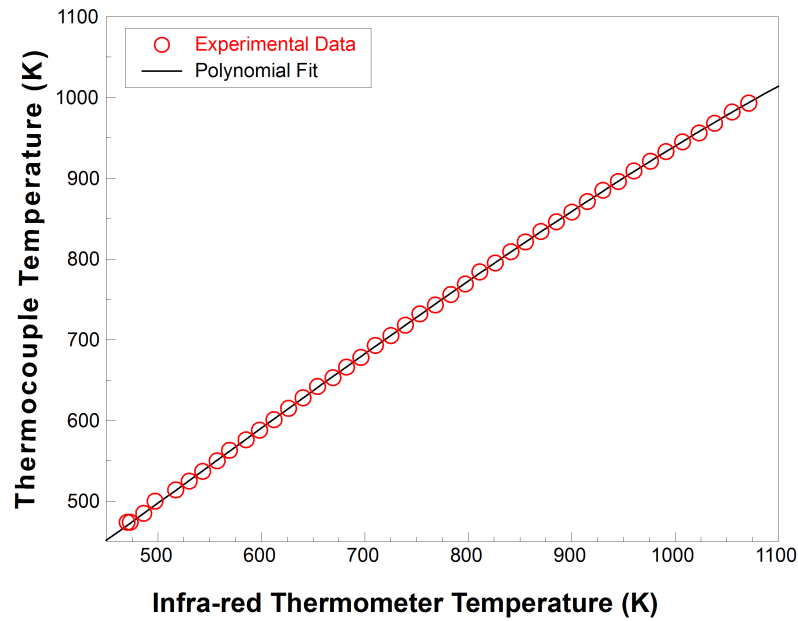
Figure 3.5: The relationship between the true temperature and the IR thermometer reading.

3.5 Analysis Procedure

After the samples were prepared, they were inserted into the AES system, sputter cleaned and annealed to 1100 K in multiple cycles at a base pressure of $< 10^{-8}$ Torr. This insured that the samples were atomically clean and that the crystalline structure was restored.

A typical analysis was done in the following manner:

- The AES system was switched on and allowed to stabilize for at least an hour and then the settings, as mentioned previously, were optimized.

- The IR Thermometer was set at a fixed distance from the sample and the measurement point centred on the sample by using the laser.

- The sample was heated to the required temperature. This was done automatically by the computer, using the output from the IR thermometer as reference.

- The sample was sputter cleaned for 400 seconds and analysis started immediately afterwards. An example of an Auger spectra before segregation can be seen in figure 3.6.

- In the case of the binary alloy, nitrogen was leaked into the system until the pressure in the chamber was $5\text{x}10^{-7}$ Torr.

- The Fe (701 eV), Mo (221 eV) and N (380 eV) peaks were continuously monitored and the analysis was stopped once equilibrium was reached.

- A complete Auger spectra was acquired to insure that no other species segregated or that oxidation has occurred. A representative example is given in figure 3.7.

3.6 Summary

In this chapter the sample preparation and experimental setup were discussed. The detail of the AES apparatus used for analysis was given, together with the equations used for quantification of a monolayer using AES. The calibration procedure of the IR thermometer, which was used to measure the surface temperature of the samples, was also discussed. The analysis procedure for acquiring the segregation profiles was given and examples of Auger spectra before and after segregation, were shown. In the next chapter the experimental results and curve fits will be discussed.
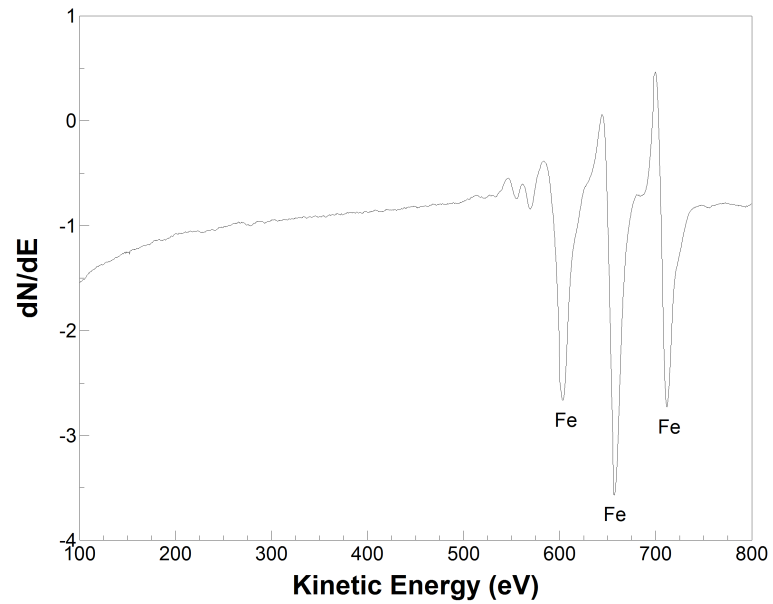
Figure 3.6: Auger spectrum before segregation has taken place at 848 K.
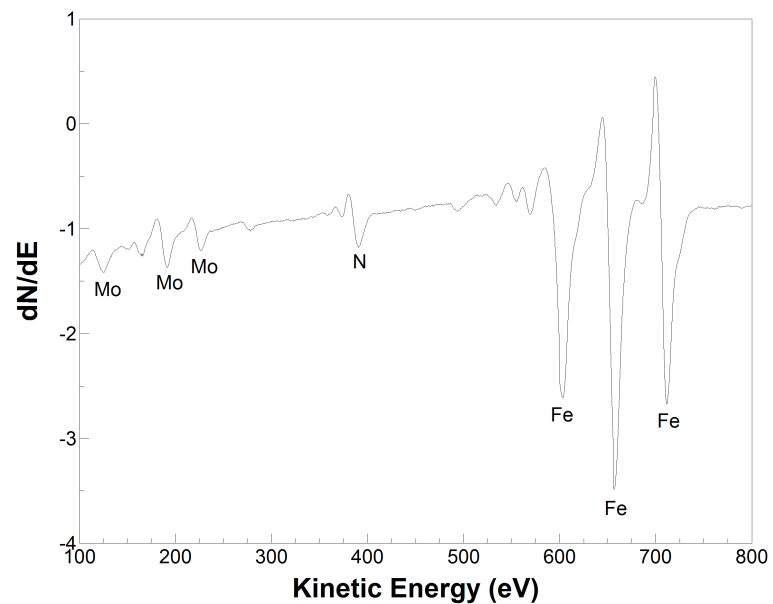
Figure 3.7: Auger spectrum after equilibrium has been reached at 848 K.

Chapter 4

Results and Discussion

4.1 Introduction

In this chapter the experimental results are discussed. Firstly, the binary system was considered. Using Fick's equation, the diffusion coefficients of molybdenum at various temperatures are determined. Taking these values and doing an Arrhenius fit, the pre-exponential factor (D_0) and activation energy (E) of molybdenum in iron are calculated. The same values are then used as initial estimates for doing the Darken curve fits. The same procedure is followed and the D_0 and E values are again calculated. In both cases it is found that the diffusion coefficient values deviate from the expected values at high temperature. By modifying the Darken model for this special case, it will be shown that there is alternative and easier method to fit the segregation profiles. It will also be shown that it corrects for the anomaly observed at the highest temperatures.

In the last part of this chapter the ternary system's results are discussed. A similar approach is taken in determining the pre-exponential factors and the activation energies E of molybdenum and nitrogen in iron using Fick's equation. Unfortunately the modified Darken approach could not be used to exactly model the ternary system. It was found that if a high diffusion coefficient (as predicted by the Fick curve fits) and low bulk concentration for nitrogen are used, that the calculations would simply take too long. However, the parameters determined by using a higher value for the nitrogen bulk concentration, were found to be realistic and it is assumed, in retrospect, that the nitrogen bulk concentration is not accurately known.

4.2 Binary system

The binary system selected for this study was a Fe-3.5wt%Mo(100) single crystal. When exposed to a nitrogen ambient of $5\text{x}10^{-7}$ Torr at temperatures ranging from 797 K to 871 K, it is observed that Mo segregates to the surface (figure 4.1). As can be seen, the Mo concentration is dependent on the N concentration and during the initial segregation up to 1000 seconds, it is observed that the Mo segregation rate (the slope of the curve) is temperature dependent, but that the nitrogen adsorption rate is almost constant for all temperatures. At equilibrium, the Mo concentration is approximately four times that of N (40 at% and 10 at%, respectively).
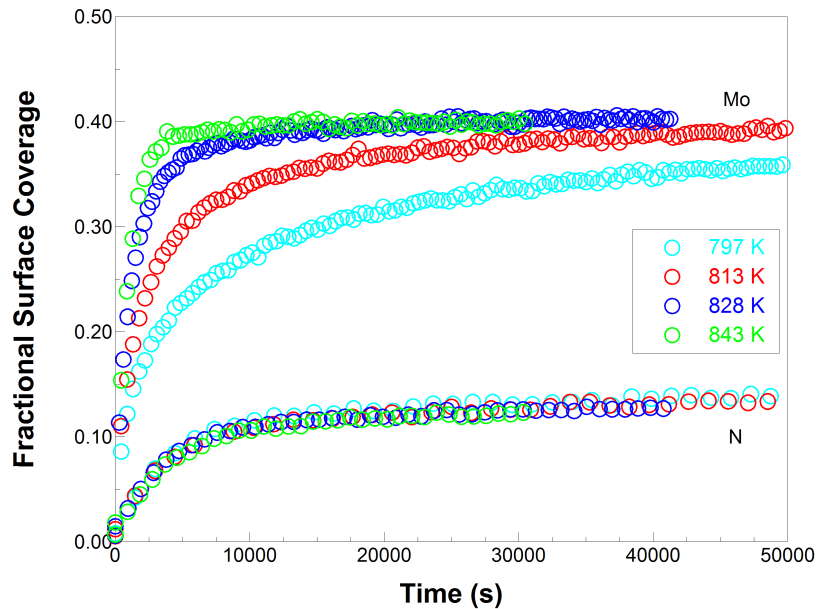
Figure 4.1: The binary system segregation profiles of Mo for the 797 - 843 K temperature range.

Fick Curve Fitting:

In chapter 2 it was shown that Fick's equation (2.4) can be used to describe the initial segregation kinetics. The experimental data curve fits were done with the *Fick Constant Temperature* software package [42] and are shown in figures 4.2 and 4.3. The values of all fitting parameters were left unchanged, except the time period over which the curve fits were done (see table 4.1). From the curve fits, the diffusion coefficients of Mo in Fe were calculated for the 813 - 871 K temperature range (also shown in table 4.1).
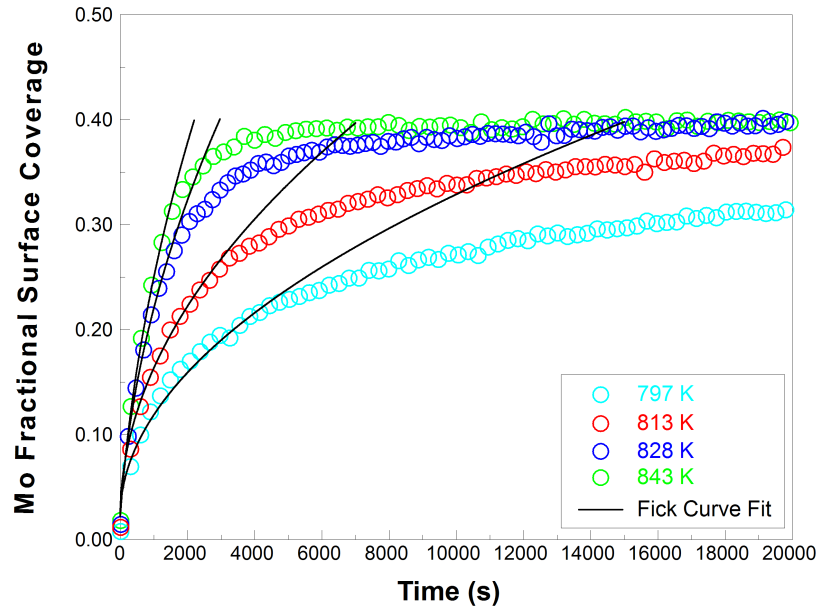
Figure 4.2: Binary system experimental data fitted using Fick's equation for the 797 - 843 K temperature range.
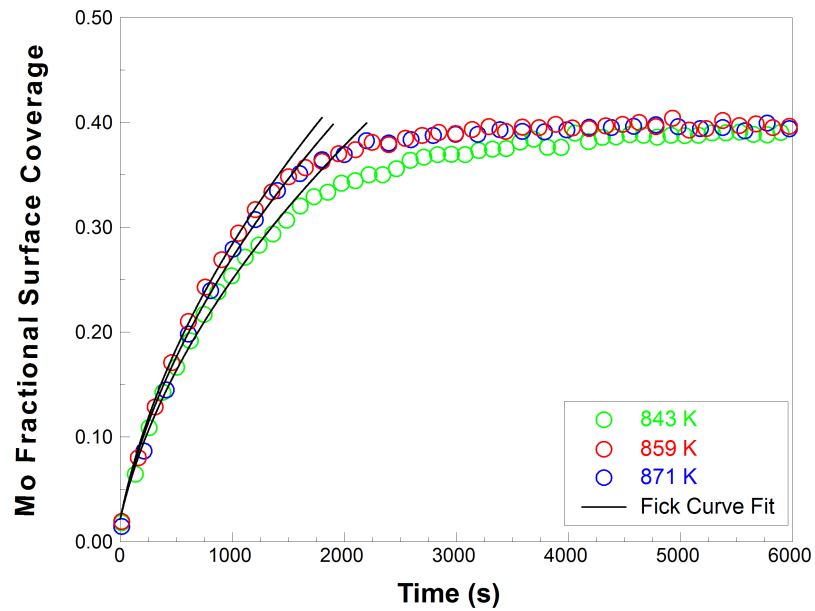

Figure 4.3: Binary system experimental data fitted using Fick's equation for the 843 - 871 K temperature range. Notice that the segregation rate for T > 850 K is not increasing.

Table 4.1: The parameters used for fitting Fick's equation to the experimental data, where T is the temperature and D is the calculated diffusion coefficient. The constant parameters were, the bulk concentration of Mo, $X_{B(Mo)} = 2.2$ at% $= 3.5$ wt%, the surface concentration of Mo after sputtering, $X_{S(Mo)} \approx 0$ and the distance between the atomic layers, $d = 2.886$ Å.

T	Fitting Range	D
(K)	(s)	$\times 10^{-21} (\mathrm{m^2/s})$
797	10-5500	1.3
813	10-2200	2.8
828	10-1500	8.9
843	10-1500	14
859	10-1200	19
871	10-1600	17
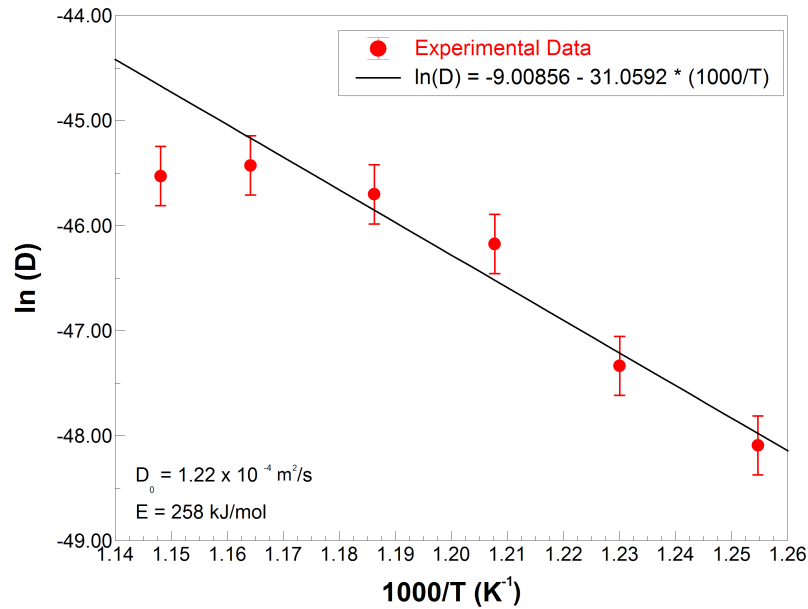
Figure 4.4: The Arrhenius plot of the Mo diffusion coefficient values determined via Fick's equation.

The calculated diffusion coefficients can be expressed in terms of temperature by the Arrhenius equation, $D = D_0 e^{-E/RT}$. A plot of $ln(D)$ against $1000/T$ is a linear function and thus the experimental data can be fitted via linear regression as shown in figure 4.4. It is observed that the data points at the highest temperatures deviate from the regression line (the reason for this behaviour will be discussed later). The linear regression resulted in the following equation:

$$ln(D) = -9.009 - 31.06 \left(\frac{1000}{T} \right) \tag{4.1}$$

From the intercept, the pre-exponential factor D_0 was calculated to be $1.2 \times 10^{-4 \pm 2}$ m^2/s and from the slope, the activation energy E was calculated to be 258 ± 33 kJ/mol.

Darken Curve Fitting:

The same experimental data was also fitted with the binary Darken model using the *Darken 2C* software package [43]. The diffusion coefficients from the previous Fick curve fits were used as approximate starting values for the Darken curve fits (as can be seen in tables 4.1 and 4.2, they are in the same order of magnitude). As can be seen in figures 4.5 and 4.6, the Darken model also describes the equilibrium conditions and the curve fits describe the experimental data very well (the curves lie on the experimental data points).

Table 4.2: The parameters used for fitting the Darken model to the experimental data, where T is the temperature, ΔG is the segregation energy and D is the calculated diffusion coefficient. The constant parameters used were, the bulk concentration of Mo, $X_{B(Mo)}$ = 2.2 at% = 3.5 wt%, the surface concentration of Mo after sputtering, $X_{S(Mo)} = 0$ and the distance between the atomic layers, d = 2.886 Å.

T (K)	ΔG (kJ/mol)	D x10^{-21}(m^2/s)
797	-31.5	1.7
813	-35	3.7
828	-35	12
843	-40	22
859	-43	55
871	-43	50

In addition to the segregation parameters that were determined by the Fick curve fits, the Darken model has the advantage of obtaining the segregation energy ΔG as well. The value was found to be in the range of -31.5 kJ/mol to -43 kJ/mol and compares favourably with the value of -15 kJ/mol determined by Uebing *et al* [9].

Figure 4.7 shows the Arrhenius plot of the diffusion coefficients that were determined (table 4.2). The linear regression line is given by

$$\ln(D) = 0.8675 - 38.83 \left(\frac{1000}{T} \right) \tag{4.2}$$

From the regression, the pre-exponential factor D_0 was determined to be $2.4 \times 10^{0 \pm 1}$ m^2/s and the activation energy E as 323 ± 16 kJ/mol. These values compare favourably with the values determined via radioactive tracer methods [44] which are 7.8×10^{-1} m^2/s and 306 kJ/mol respectively.
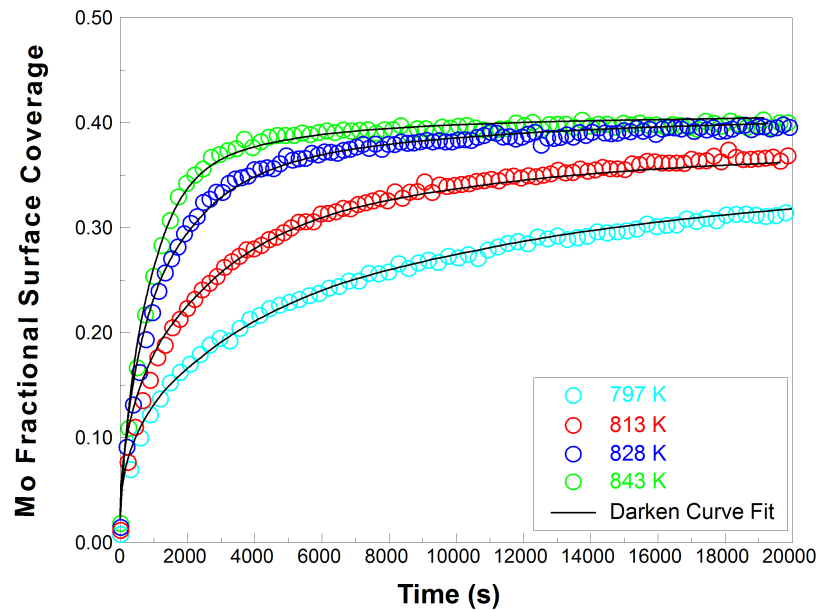
Figure 4.5: The binary system Darken curve fits of the experimental data for 797 - 843 K temperature range.
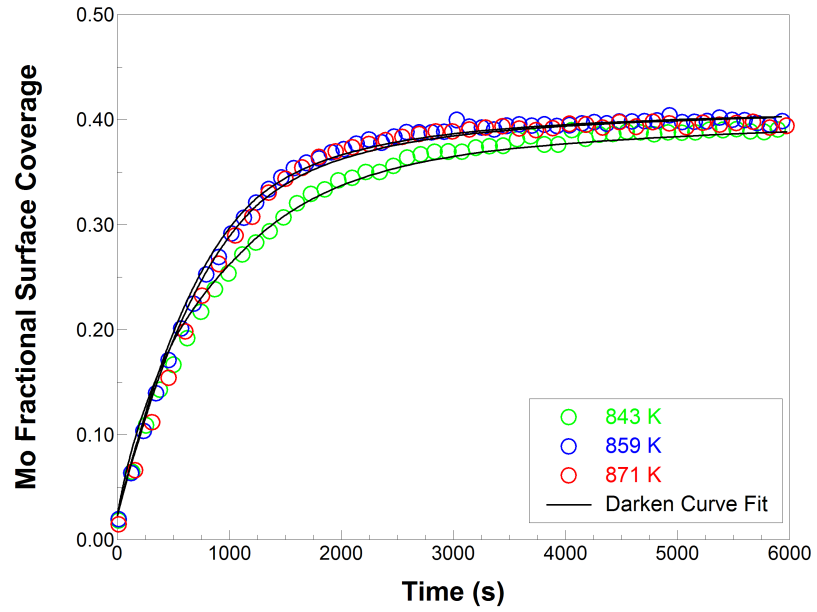
Figure 4.6: The binary system Darken curve fits of the experimental data for 843 - 871 K temperature range.
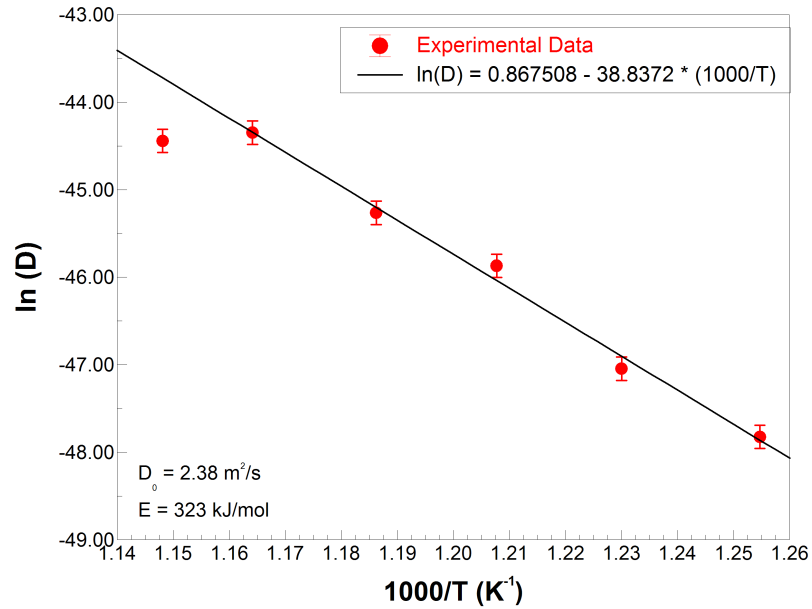

Figure 4.7: The Arrhenius plot of the diffusion coefficient values determined via the Darken model.

The special case of a binary bulk and ternary surface:

In the previous curve fits and Arrhenius plots it is observed that the segregation rate of Mo at temperatures higher than 850K was not increasing as expected. As was shown in section 2.3.2 this is a special case in which the adsorption of nitrogen becomes the limiting factor for the molybdenum segregation rate. At these conditions it can be safely assumed that the Mo and N are in equilibrium at the surface and thus the following equation was derived:

$$\Delta G'(N)_{Mo} = -RT \ln \left(\frac{X_{Mo}^{\phi}(1 - X_{Mo}^{B})}{X_{Mo}^{B}(1 - X_{Mo}^{\phi})} \right) \tag{4.3}$$

All the variables on the right-hand side of the equation are known and by plotting $\Delta G'(N)_{Mo}$ against X_N^{ϕ} as shown in figure 4.8, an expression can be derived for $\Delta G'(N)_{Mo}$ via a polynomial curve fit as follows:

$$\Delta G(N)_{Mo} = -1.74 - 3.20\text{x}10^3(\text{X}_N^{\phi}) + 9.07\text{x}10^4(\text{X}_N^{\phi})^2$$
$$-1.31\text{x}10^6(\text{X}_N^{\phi})^3 + 9.59\text{x}10^6(\text{X}_N^{\phi})^4 - 2.78\text{x}10^7(\text{X}_N^{\phi})^5 \tag{4.4}$$

By making a small modification to the fitting software, the abovementioned polynomial fit was included in the algorithms and the curve fits as seen in figure 4.9 were generated by changing only one parameter, the diffusion coefficient D (refer to table 4.3). Although the difference between the two curve fits at 859 K and 871 K still seems negligible, the differences in their diffusion coefficients are significant.

The Arrhenius plot of the D values is shown in figure 4.10. Note that the data point for 871 K is pulled back onto the Arrhenius regression line which is given by

$$\ln(D) = 4.001 - 41.55 \left(\frac{1000}{T} \right) \tag{4.5}$$

From the linear regression, the pre-exponential factor D_0 was calculated as $5.5\text{x}10^{1\pm1}$ m^2/s and the activation energy E as 345 ± 18 kJ/mol.

Table 4.3: The diffusion coefficient values used for fitting the Darken model using the segregation energy equation 4.4, where T is the temperature. The constant parameters were, the bulk concentration of Mo, $X_{B(Mo)} = 2.2$ at% $= 3.5$ wt%, the surface concentration of Mo after sputtering, $X_{S(Mo)} \approx 0$ and the distance between the atomic layers, $d = 2.886$ Å.

T (K)	D x10^{-21} (m^2/s)
828	9.0
843	20
859	60
871	100
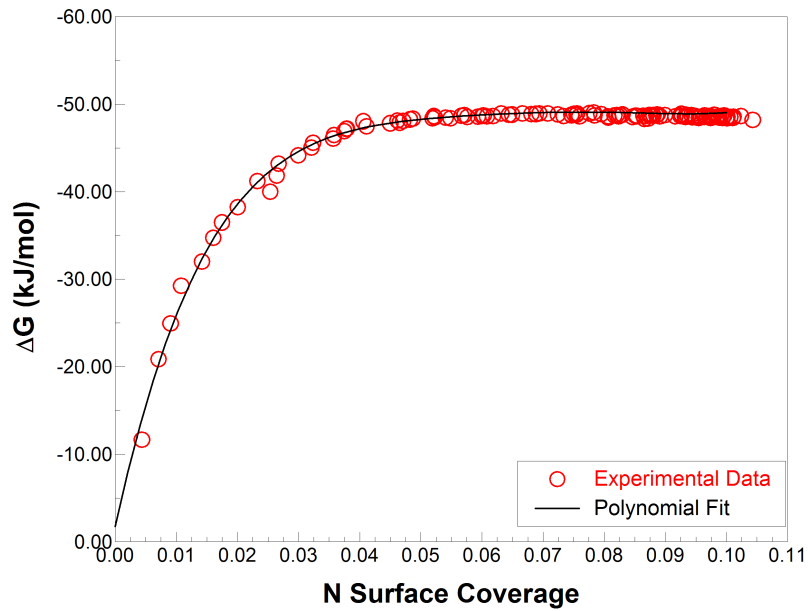
Figure 4.8: The segregation energy $\Delta G'(N)_{Mo}$ as a function of the nitrogen surface concentration X_N^ϕ.
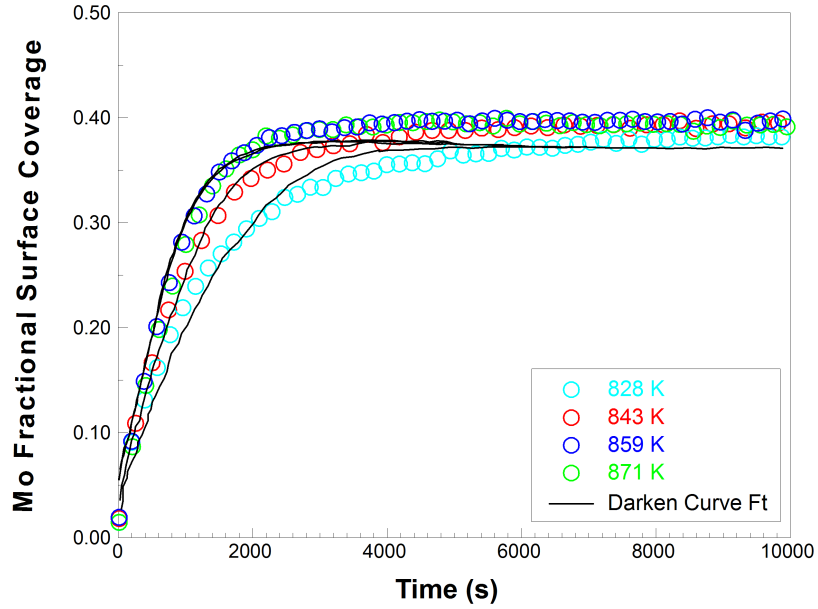
Figure 4.9: The Darken curve fits using the $\Delta G'(N)_{Mo}$ as determined via equation 4.3.
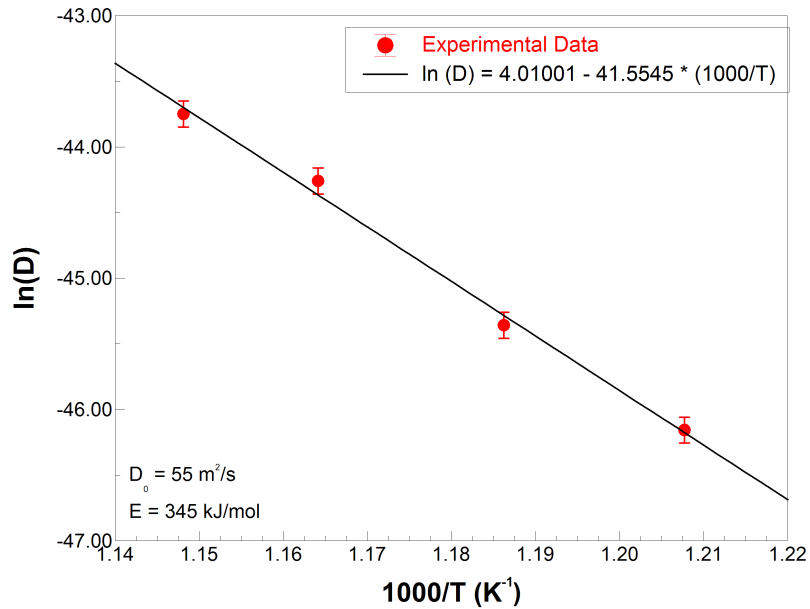
Figure 4.10: The Arrhenius plot of the diffusion values in table 4.3.

4.3 Ternary system

The ternary system analysed in this study was a Fe-3.5wt%Mo(100)-N single crystal. When exposed to high temperatures ranging from 828 K to 888 K, it is observed that Mo and N co-segregate to the surface as can be seen in figure 4.11. While the two species depend on each other to segregate, it is observed that the segregation rate of nitrogen is considerably higher. At equilibrium, the Mo concentration is 50 at% and the N concentration is 25 at%, or in other words the Mo to N ratio is 2:1.
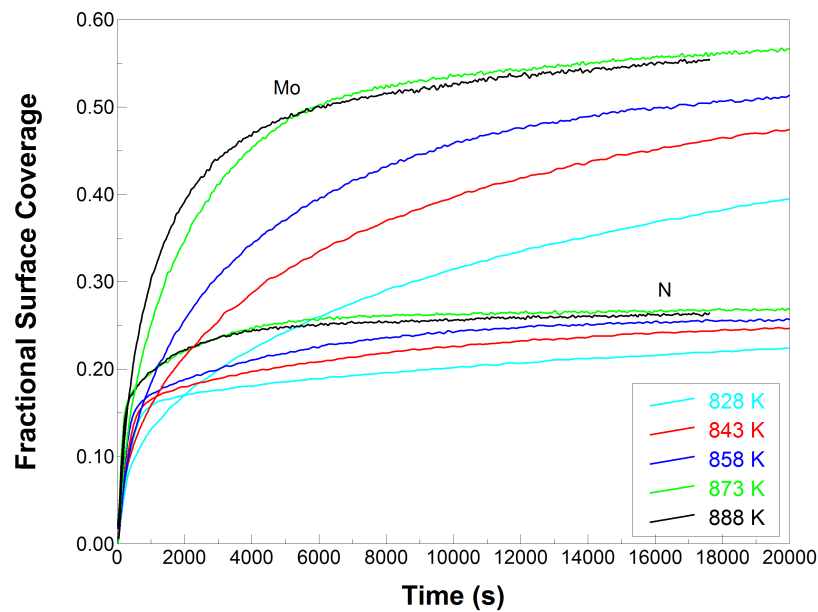
Figure 4.11: The ternary system segregation profiles of Mo and N for the 828 - 888 K temperature range.

Fick Curve Fitting:

Though Fick's equation does not describe co-segregation as it is assumed that surface species do not interact with each other, it is still useful in determining the diffusion coefficients of the segregating species as shown in figures 4.12 and 4.13. The fits were done with the *Fick Constant Temperature* software package [42] and the D values of Mo and N determined thus are shown in table 4.4. The Arrhenius plots of the two species are shown in figures 4.14 and 4.15. From the linear regressions the pre-exponential factor for Mo was calculated as $3.6 \times 10^{-2 \pm 1}$ m^2/s and for N it was found to be $4.1 \times 10^{-1 \pm 2}$ m^2/s. The activation energies were calculated as 308 ± 20 kJ/mol and 210 ± 40 kJ/mol for Mo and N, respectively.

Table 4.4: The parameters used for fitting Fick's equation to the experimental data, where T is the temperature and D_i is the calculated diffusion coefficient of species i. The constant parameters were, the bulk concentration of Mo, $X_B^{Mo} = 2.2$ at% $= 3.5$wt %, the bulk concentration of N, $X_B^N = 0.0015$ at% and the distance between the atomic layers, $d = 2.886$ Å.

T (K)	D_{Mo} x10^{-21}(m^2/s)	D_N x10^{-14}(m^2/s)
828	1.5	2.4
843	2.5	3.9
858	5.6	5.3
871	15	17
888	28	15
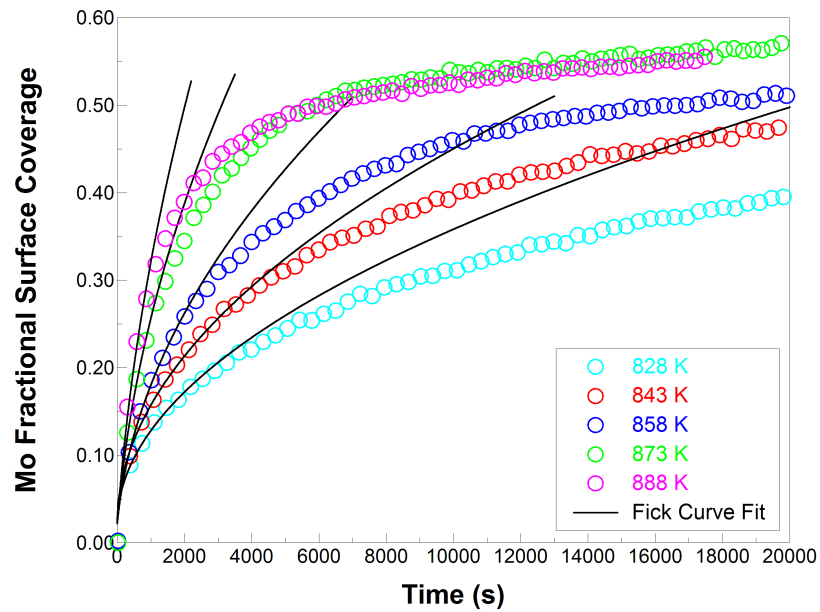
Figure 4.12: The ternary system Fick curve fits of the Mo experimental data for the 828 - 888 K temperature range.
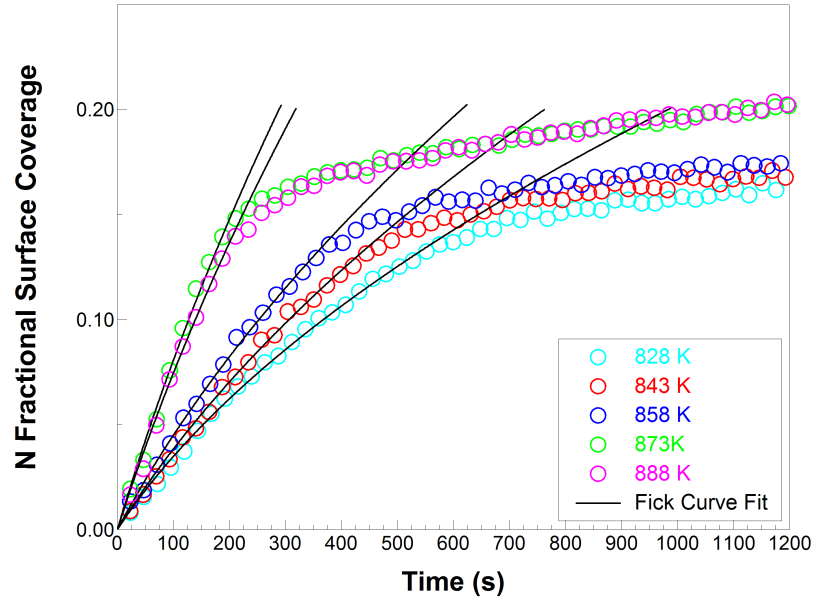
Figure 4.13: The ternary system Fick curve fits of the N experimental data for the 828 - 888 K temperature range.
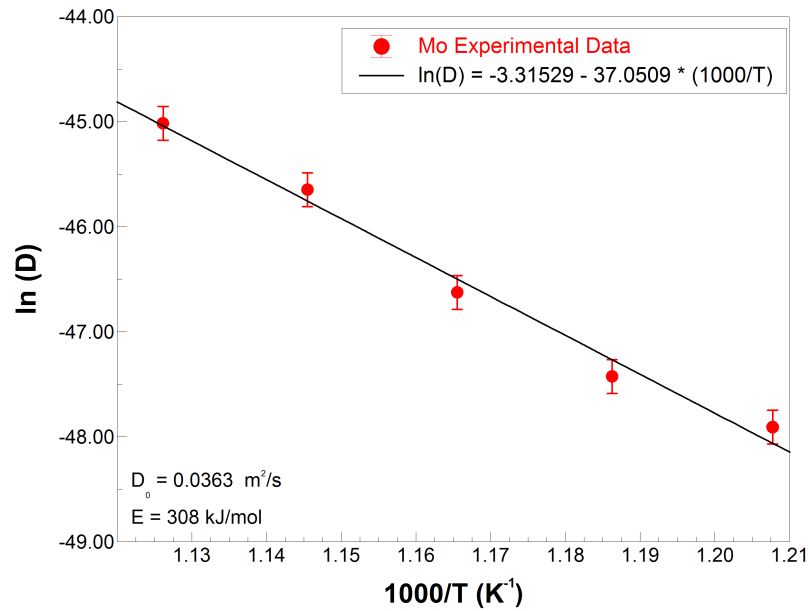

Figure 4.14: The Arrhenius plot of the Mo experimental data fitted using Fick's equation.
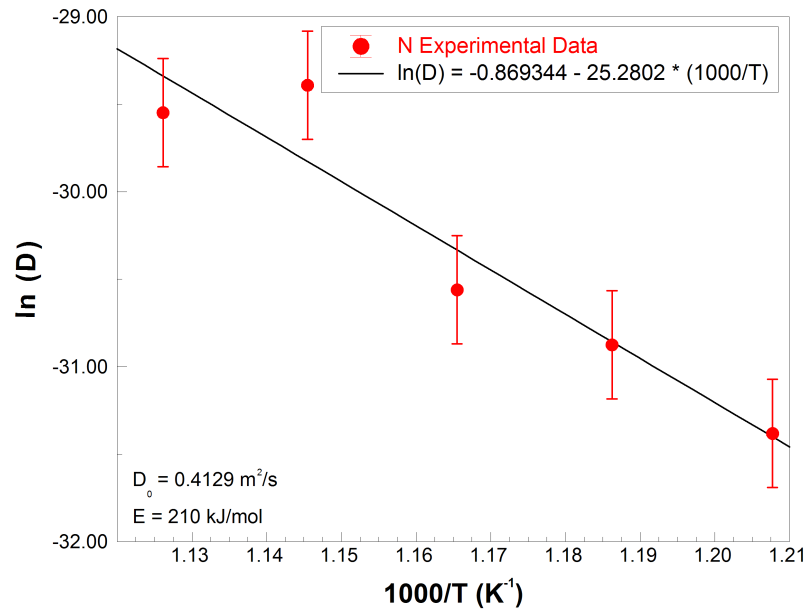
Figure 4.15: The Arrhenius plot of the N experimental data fitted using Fick's equation.

Darken Curve Fitting:

The ternary system experimental data was also fitted by the modified Darken approach using the *Darken 3C* software package [15]. The parameters used for the curve fits are shown in table 4.5. For the sake of clarity the curve fits are shown individually in figures 4.16 to 4.20. It was found that if a low bulk concentration for nitrogen was used, that the experimental data could not be fitted. Therefore a value of 2.0 at% was used.

As mentioned before, the Darken model describes both the kinetics and equilibrium and in the case of the ternary system, additional information is acquired, namely the segregation energies of Mo and N, ΔG_{Mo} and ΔG_N, as well as the interaction coefficient between the two species $\Omega_{Mo,N}$. The average ΔG_{Mo} value was determined to be -32 kJ/mol and -19 kJ/mol for ΔG_N. The average interaction coefficient $\Omega_{Mo,N}$ was determined to be -19 kJ/mol.

The Arrhenius plots for the Mo and N diffusion coefficients are shown in figures 4.21 and 4.22. From the linear regressions, the activation energies for Mo and N in Fe, were calculated as 271±11 kJ/mol and 323±43 kJ/mol, respectively. The pre-exponential factors were calculated as $1.9 \times 10^{-4\pm1}$ m^2/s and $2.8 \times 10^{0\pm3}$ m^2/s.

Table 4.5: The parameters used for fitting the ternary Darken model to the experimental data, where T is the temperature, ΔG_i is the segregation energy of species i, D_i is the calculated diffusion coefficient of species i and $\Omega_{Mo,N}$ is the interaction coefficient between Mo and N. The constant parameters used were, the bulk concentration of Mo, $X_B^{Mo} = 2.2$ at% = 3.5 wt%, the bulk concentration of N, $X_B^N = 2.0$ at%, the interaction coefficient between the segregating species and bulk $\Omega_{(1/2,3)} = 0$ kJ/mol and the distance between the atomic layers, $d = 2.886$ Å.

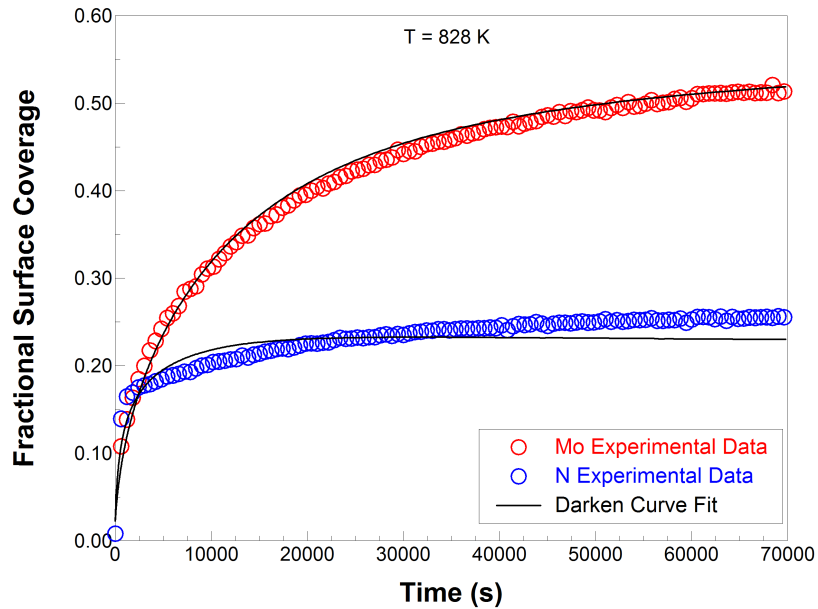| T (K)	ΔG_{Mo} (kJ/mol)	ΔG_N (kJ/mol)	D_{Mo} x10^{-21}(m^2/s)	D_N x10^{-20}(m^2/s)	$\Omega_{Mo,N}$ (kJ/mol)
828	-31	-18	1.5	1.0	-18
843	-32	-19	3.0	3.0	-18
858	-32	-19	6.0	7.0	-18
871	-34	-20	13	20	-20
888	-33	-20	20	20	-20

Figure 4.16: The ternary system Darken curve fit for T = 828 K.
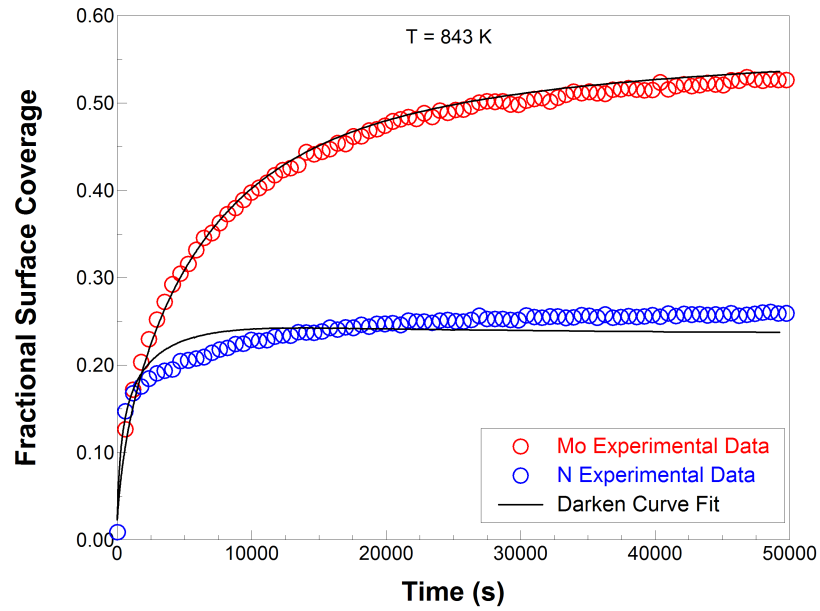
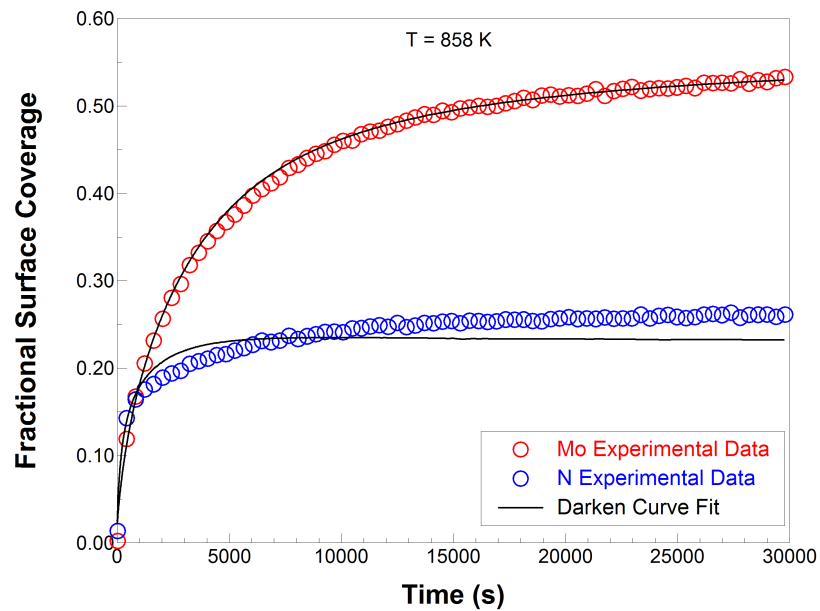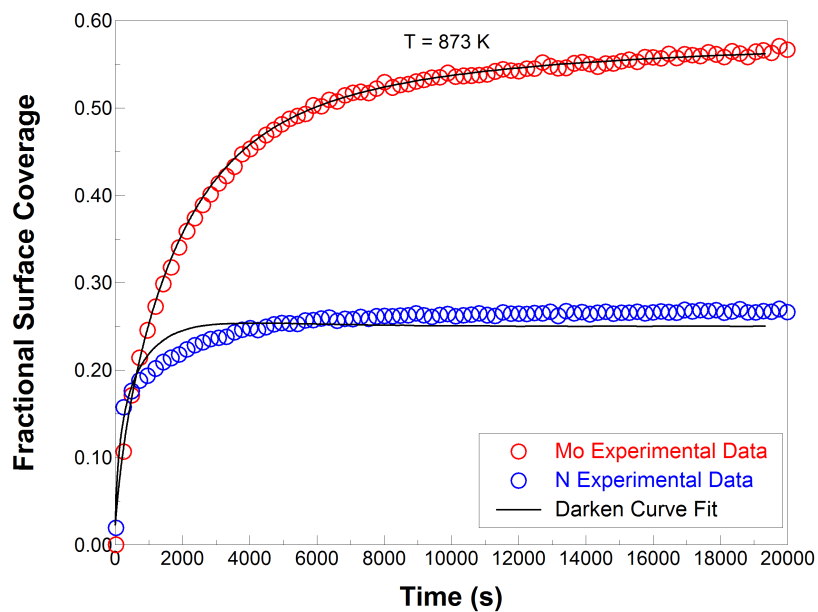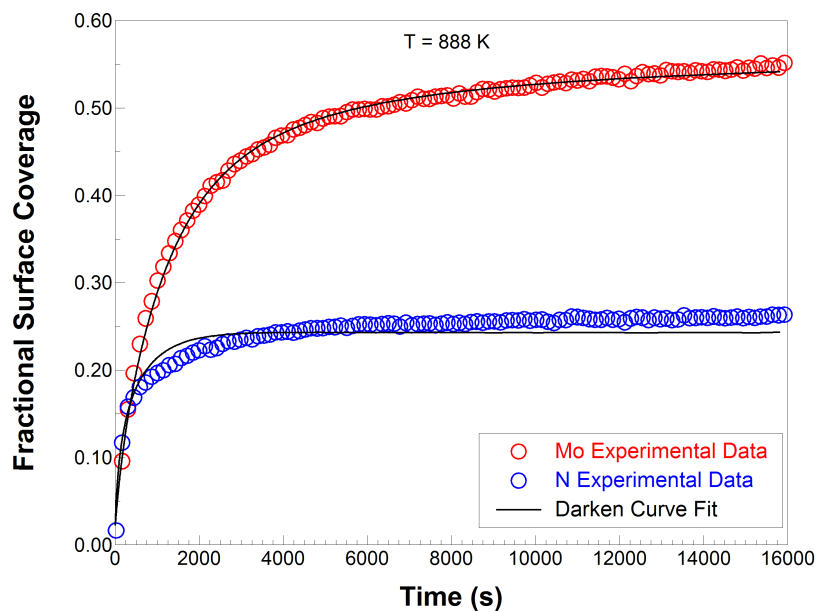Figure 4.17: The ternary system Darken curve fit for T = 843 K.

Figure 4.18: The ternary system Darken curve fit for T = 858 K.

Figure 4.19: The ternary system Darken curve fit for T = 873 K.

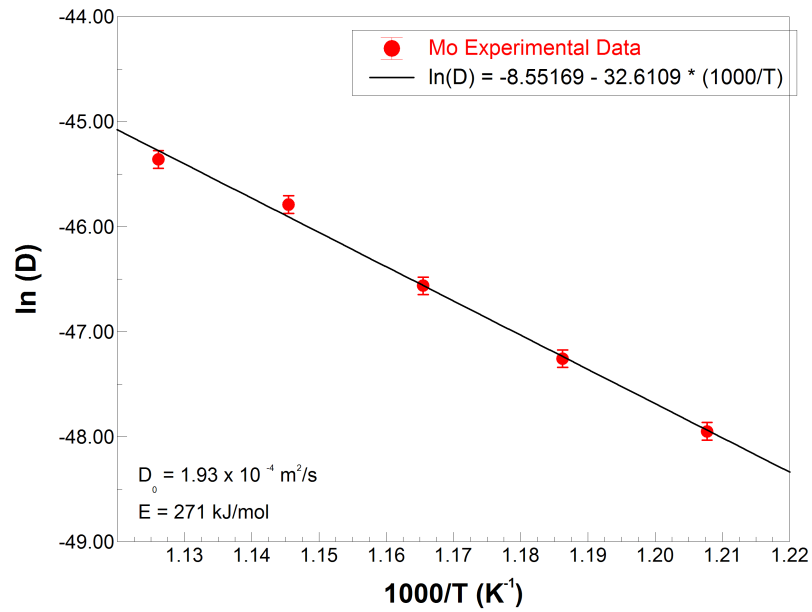Figure 4.20: The ternary system Darken curve fit for T = 888 K.

Figure 4.21: The Arrhenius plot for the Mo diffusion coefficients determined via the modified Darken approach.
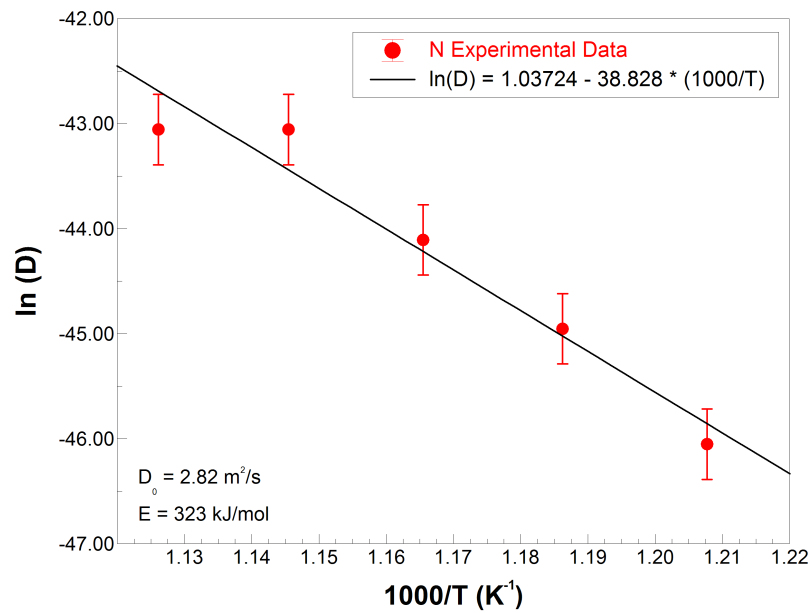

Figure 4.22: The Arrhenius plot for the N diffusion coefficients determined via the modified Darken approach.

4.4 Summary

In this chapter the experimental segregation profiles, acquired by Auger Electron Spectroscopy, for the binary and ternary systems were shown. Fick's equation and the modified Darken approach were used to obtain curve fits for the segregation profiles and subsequently the diffusion coefficient values, D_{Mo} and D_N, were determined at various temperatures. Using the linear regression technique, the pre-exponential factors D_0 and activation energies E of Mo and N in Fe were calculated for all the methods that were used. The Darken method was used to obtain additional information about the systems, namely the segregation energies ΔG of Mo and N and the interaction coefficient Ω between the segregating species. In the next chapter, a conclusive summary of all the results is given.

Chapter 5

Conclusive Summary

The segregation parameters determined for the binary and ternary systems are summarized in table 5.1. For comparison, the Arrhenius linear regression lines of Mo are also shown in figure 5.1. As can be seen in table 5.1, the D_0 values of Mo vary between 1.2×10^{-4} m^2/s and 5.5×10^1 m^2/s and the E values, between 258 kJ/mol and 345 kJ/mol. These values are comparable to 7.8×10^{-1} m^2/s and 306 kJ/mol, determined via radioactive tracer methods [44].

Table 5.1: A summary of the segregation parameters determined for the two systems via Fick's equation and the modified Darken approach.

System	Method	Species	D_0 (m^2/s)	E (kJ/mol)	ΔG (kJ/mol)	$\Omega_{Mo,N}$ (kJ/mol)
Binary	Fick	Mo	$1.2 \times 10^{-4 \pm 2}$	258±33		
	Darken	Mo	$2.4 \times 10^{0 \pm 1}$	323±16	-38	
	Special Case	Mo	$5.5 \times 10^{1 \pm 1}$	345±18	Polynomial	
Ternary	Fick	Mo	$3.6 \times 10^{-2 \pm 1}$	308±20		
		N	$4.1 \times 10^{-1 \pm 2}$	210±40		
	Darken	Mo	$1.9 \times 10^{-4 \pm 1}$	271±11	-32	-19
		N	$2.8 \times 10^{0 \pm 3}$	323±43	-19	
	Other	Mo	7.8×10^{-1}[44]	306	-15[9];-28[45]	-35[9]
	Methods	N	4.7×10^{-4}[46]	77		

56

Referring to figure 5.1, it is encouraging to see the regression lines overlap, even though different models and different physical samples were investigated. Using the Darken model, the segregation energy of Mo was also determined. In the case of the binary system it was found to be -38 kJ/mol. Maruyama *et al* found it to be -28 kJ/mol using the Langmuir-McLean equilibrium method. For the ternary system it was calculated as -32 kJ/mol and Uebing *et al* found it to be -15 kJ/mol, also using equilibrium studies.

It was found that the pre-exponential factors determined for nitrogen via Fick's equation and the Darken approach, are in the same order of magnitude, i.e. 4.1×10^{-1} m^2/s and 2.82 m^2/s, respectively. The activation energies, in these cases, were found to be 210 kJ/mol and 323 kJ/mol. The values determined via other methods are given in Askeland [46] as 4.7×10^{-4} m^2/s and 77 kJ/mol. The segregation energy of N was determined by the Darken model as -19 kJ/mol. The interaction coefficient between Mo and N was determined as -19 kJ/mol. This value compares favourably with the value of -35 kJ/mol determined by Uebing *et al* [11].
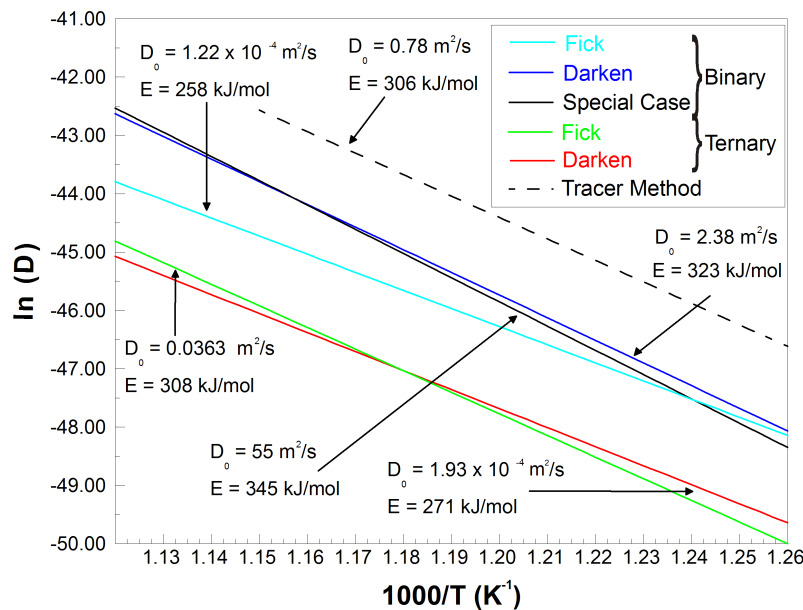

Figure 5.1: The Arrhenius linear regression lines of Mo for the different methods applied during the study of the binary and ternary systems.

Bibliography

[1] WMH Sachtler and RA van Santen, Appl. Surf. Sci., 3 (1979) 121

[2] Y Samson *et al*, Appl. Surf. Sci., 72 (1993) 373

[3] MS Spencer, Surf. Sci., 192 (1987) 336

[4] AG Guy, Introduction to Materials Science, First edition, 1972

[5] AG Guy, Essentials of Materials Science, First edition, 1976

[6] D McLean, Grain Boundaries in Metals, Oxford University Press, London, 1957

[7] D McLean and L Northcott, J. Iron Steel Inst., 158 (1948) 169

[8] J Crank, The Mathematics of Diffusion, 2nd Edition, 1975

[9] B Eltester and C Uebing, Surf. Sci., 347 (1996) 39-45

[10] A Baraldi, B Brena, D Cocco, G Comelli, D Lizzit, G Paolucci, P Baumann, V Scheuch and C Uebing, Vacuum, 47 (1997) 351-355

[11] C Uebing and EC Viljoen, Surf. Sci., 410 (1998) 123-131

[12] J Woodward and GT Burstein, Met. Sci., 14 (1980) 529

[13] C Lea and MP Seah, Scripta Metall., 9 (1975) 583

[14] M Guttman, Surf. Sci., 53 (1975) 213

[15] JJ Terblans, *Darken 3C* fitting software, University of the Free State

[16] J du Plessis, Diffusion and Defect Data B, 10 (1990)

[17] J du Plessis, PE Viljoen and GN van Wyk, Surf. Sci., 244 (1991) 277

[18] CHP Lupis, Chemical Thermodynamics of Materials, North-Holland, Amsterdam, 1983

[19] LS Darken, Trans. AIME, 180 (1949) 430

[20] J du Plessis and GN van Wyk, J. Phys. Chem. Solids, 50 (1989) 277

[21] NAG Routines Mark 11, Numerical Algorithm Group, Oxford

[22] CJ McMahon and L Marchut, J. Vac. Sci. Technol., 15 (1978) 450

[23] EC Viljoen, WA Jordaan and J du Plessis, Vacuum, 61 (2001) 141

[24] MP Seah, J. Micros. and Spectrosc. Electron., 8 (1983) 177

[25] A Siokou, S Kennou and S Ladas, Surf. Sci., 307-309 (1994) 810

[26] DJ O'Conner, HJ Kang, P Pigram, RH Roberts and S He, Appl. Surf. Sci., 70/71 (1993) 114

[27] D Ren and TT Tsong, Surf. Sci., 184 (1987) L439

[28] S Hofmann, Vacuum, 40 (1990) 9

[29] Auger and X-ray Photoelectron Spectroscopy, D Briggs and MP Seah (eds.), 2nd edition, John Wiley & Sons Inc., 1990

[30] JJ Gilman, The Art and Science of Growing Crystals, John Wiley &Sons Inc., 1963

[31] JJ Terblans, M.Sc. Thesis, University of the Free State, 1997

[32] MP Seah, *Quantification of AES and XPS* in Practical Surface Analysis, Volume 1, D Briggs and MP Seah (eds.), 2nd edition, John Wiley & Sons Inc., 1990

[33] J du Plessis, Surf. and Interf. Anal., 20 (1993) 228

[34] MP Seah, Surf. and Interf. Anal., 21 (1994) 587

[35] J du Plessis, Surf. and Interf. Anal., 21 (1994) 590

[36] Handbook of Auger Electron Spectroscopy, Ed. CL Hedberg, Physical Electronics Inc., Eden Prairie, MN, 1995

[37] R Shimizu, J of Appl. Phys., 22 (1983) 1631

[38] S Tanuma, CJ Powell and DR Penn, Surf. and Interf. Anal., 17 (1991) 911

[39] BD Cullity, Elements of X-ray diffraction, 2nd edition, Addison-Wesley Publishing Company Inc., 1978

[40] RC Weast, Handbook of Chemistry and Physics, CRC Press, (1984) E48

[41] J Holman, Experimental Methods for Engineers, McGraw-Hill, (1984) 299

[42] JJ Terblans, *Fick Constant Temperature* fitting software, University of the Free State

[43] JJ Terblans, *Darken 2C* fitting software, University of the Free State

[44] DR Lide, Handbook of Chemistry and Physics, CRC Press, New York, (1997) F-54

[45] N Maruyama, GDW Smith and A Cerezo, Mat. Sci. and Eng., A353 (2003) 126

[46] D Askeland, The Science and Engineering of Materials, Third Edition, Chapman and Hall, 1996